Contrib Mineral Petrol
DOI 10.1007/s00410-008-0330-0

ORIGINAL PAPER

The origin of hydrous, high-$\delta^{18}O$ voluminous volcanism: diverse oxygen isotope values and high magmatic water contents within the volcanic record of Klyuchevskoy volcano, Kamchatka, Russia

Sara Auer · Ilya Bindeman · Paul Wallace · Vera Ponomareva · Maxim Portnyagin

Received: 14 February 2008 / Accepted: 17 July 2008

Abstract Klyuchevskoy volcano, in Kamchatka's subduction zone, is one of the most active arc volcanoes in the world and contains some of the highest $\delta^{18}O$ values for olivines and basalts. We present an oxygen isotope and melt inclusion study of olivine phenocrysts in conjunction with major and trace element analyses of ^{14}C- and tephrochronologically-dated tephra layers and lavas spanning the eruptive history of Klyuchevskoy. Whole-rock and groundmass analyses of tephra layers and lava samples demonstrate that both high-Mg (7–12.5 wt% MgO) and high-Al (17–19 wt% Al_2O_3, 3–6.5 wt% MgO) basalt and basaltic andesite erupted coevally from the central vent and flank cones. Individual and bulk olivine $\delta^{18}O$ range from normal MORB values of 5.1‰ to values as high as 7.6‰. Likewise, tephra and lava matrix glass have high-$\delta^{18}O$ values of 5.8–8.1‰. High-Al basalts dominate volumetrically in Klyuchevskoy's volcanic record and are mostly high in $\delta^{18}O$. High-$\delta^{18}O$ olivines and more normal-$\delta^{18}O$ olivines occur in both high-Mg and high-Al samples. Most olivines in either high-Al or high-Mg basalts are not in oxygen isotopic equilibrium with their host glasses, and $\Delta^{18}O_{olivine-glass}$ values are out of equilibrium by up to 1.5‰. Olivines are also out of Fe–Mg equilibrium with the host glasses, but to a lesser extent. Water concentrations in olivine-hosted melt inclusions from five tephra samples range from 0.4 to 7.1 wt%. Melt inclusion CO_2 concentrations vary from below detection (<50 ppm) to 1,900 ppm. These values indicate depths of crystallization up to ~17 km (5 kbar). The variable H_2O and CO_2 concentrations likely reflect crystallization of olivine and entrapment of inclusions in ascending and degassing magma. Oxygen isotope and Fe–Mg disequilibria together with melt inclusion data indicate that olivine was mixed and recycled between high-Al and high-Mg basaltic melts and cumulates, and Fe–Mg and $\delta^{18}O$ re-equilibration processes were incomplete. Major and trace elements in the variably high-$\delta^{18}O$ olivines suggest a peridotite source for the parental magmas. Voluminous, highest in the world with respect to $\delta^{18}O$, and hydrous basic volcanism in Klyuchevskoy and other Central Kamchatka depression volcanoes is explained by a model in which the ascending primitive melts that resulted from the hydrous melt fluxing of mantle wedge peridotite, interacted with the shallow high-$\delta^{18}O$ lithospheric mantle that had been extensively hydrated during earlier times when it was part of the Kamchatka forearc. Following accretion of the Eastern Peninsula terrains several million years ago, a trench jump eastward caused the old forearc mantle to be beneath the presently active arc. Variable interaction of ascending flux-melting-derived melts with this older, high-$\delta^{18}O$ lithospheric mantle has produced mafic parental magmas with a spectrum of $\delta^{18}O$ values. Differentiation of the higher $\delta^{18}O$ parental magmas has created the volumetrically dominant high-Al basalt series.

Communicated by T.L. Grove.

Electronic supplementary material The online version of this article (doi:10.1007/s00410-008-0330-0) contains supplementary material, which is available to authorized users.

S. Auer · I. Bindeman (✉) · P. Wallace
Department of Geological Sciences, 1272 University of Oregon, Eugene, OR 97403, USA
e-mail: bindeman@uoregon.edu

V. Ponomareva
Institute of Volcanology and Seismology, 9 Piip Boulevard, Petropavlovsk-Kamchatsky 683006, Russia

M. Portnyagin
IFM-GEOMAR Leibniz Institute for Marine Sciences, The University of Kiel, Wischhofstrasse 1-3, 24148 Kiel, Germany

Both basalt types incessantly rise and mix between themselves and with variable in $\delta^{18}O$ cumulates within dynamic Klyuchevskoy magma plumbing system, causing biannual eruptions and heterogeneous magma products.

Keywords Oxygen isotopes · Olivine · Melt inclusions · Hydrous melting · Ion microprobe

Introduction: geologic overview of the Kamchatka Peninsula

Tectonic history of Kamchatka

The Kamchatka Peninsula is an active component of the circumpacific volcanism (Fig. 1). The area has had a complex accretionary history characterized by eastward growth and migration of the volcanic front (Konstantinovskaia 2000; Bindeman et al. 2002; Lander and Shapiro 2007). Since the Late Eocene the accreted terrain of the Sredinny Range was the locality of the volcanic front. Accretion of the Eastern Kamchatka intra-oceanic terrain and the Pliocene accretion of cape-peninsulas onto Eastern Kamchatka (e.g., Lander and Shapiro 2007), resulted in locking of the subduction zone, breaking-off and sinking of the subducting Kula plate, with subsequent subduction zone migrating to the East, to its present location. This transition initiated the formation of the Eastern volcanic front (EVF) and volcanic zone of the Central Kamchatka depression (CKD) (Fig. 1), while the former volcanic front on Sredinny Range diminished its activity.

Volcanism patterns reflect Kamchatka's Eocene-present tectonic history (e.g., Avdeiko et al. 2007) and are expressed in three main volcanic belts (Fig. 1): the Sredinny Range, the EVF, and the CKD. The CKD, a 200-km wide graben-like feature, is home to some of the most active of arc volcanoes in the world.

The voluminous volcanism in the CKD was proposed to result from partial melting of and fluid release from the subducted, thick, hydrated crust of the Hawaii-Emperor

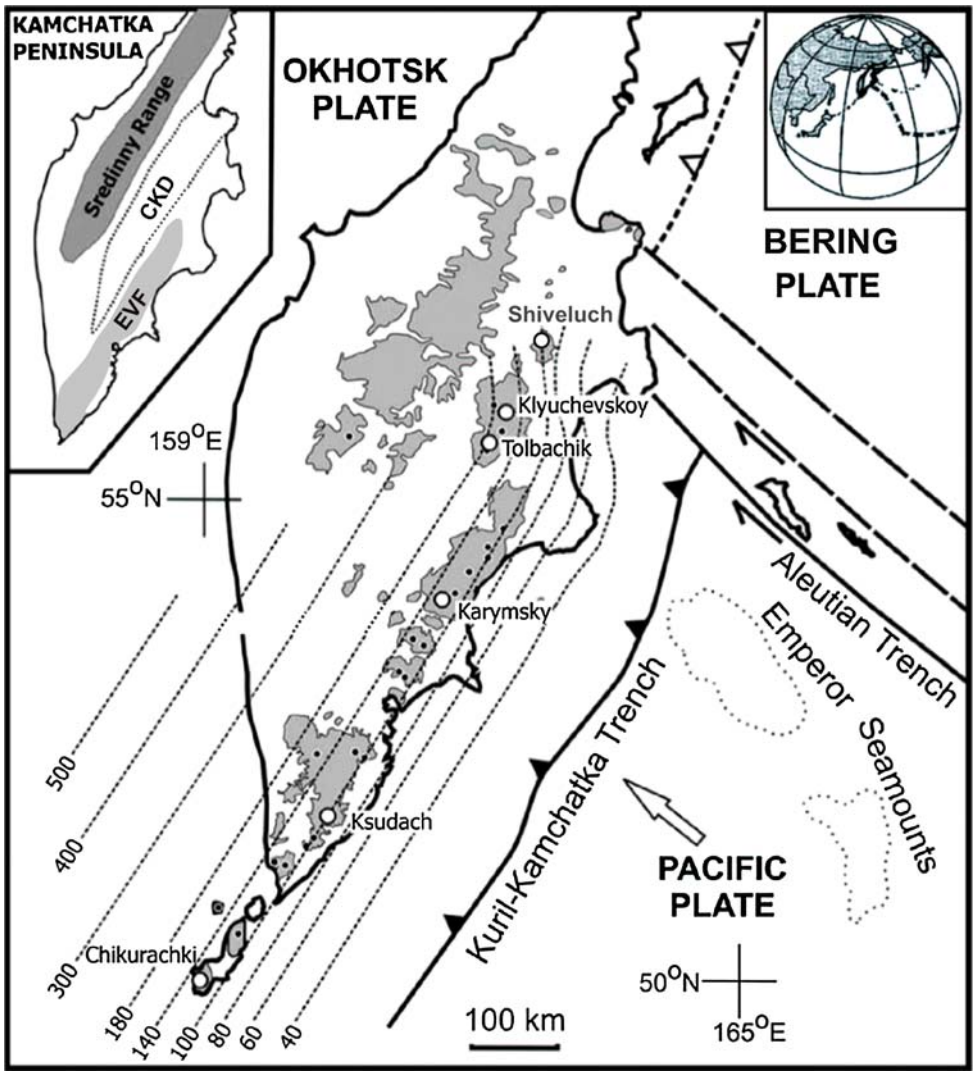

Fig. 1 Tectonic position and main volcanic zones of the Kamchatka Peninsula, NW Pacific. *Gray areas* show main volcanic fields; active volcanoes are shown with *black dots and white circles*. *Dashed lines* are isodepth contours (km) approximating the upper surface of the subducting Pacific plate (Gorbatov et al. 1997). *Inset in upper right corner* shows global position of Kamchatka and Hawaii-Emperor island chain. *Inset in upper left corner* shows Kamchatka major volcanic zones: Sredinny Ridge, Central Kamchatka depression (CKD), and Eastern volcanic front (EVF). Klyuchevskoy volcano is located in the Central Kamchatka depression, close to the Kamchatka-Aleutian junction

Seamount chain (Volynets 1994; Kersting and Arculus 1994; Dorendorf et al. 2000). Alternatively, an episode of "catastrophic slab loss" in the Pliocene (e.g., Levin et al. 2002; Portnyagin et al. 2005), in which a portion of the subducted slab broke off and sank into the mantle, could have caused upwelling of hot mantle, and extensive melting of hydrated asthenosphere, and/or lower crust. Finally, mantle edge flow can explain slab melting and voluminous adakitic volcanism at northern CKD volcanoes (e.g., Yogodzinski et al. 2001).

The Pacific plate is subducting under Kamchatka at a fast rate of ~7–8 cm/year at a slab angle of about 55°, which shallows to the north to around 25° (Fig. 1; Gorbatov et al. 1997, 1999). This has important implications for mantle wedge thermal structure, which affects magma compositions and magmatic flux along the CKD (Portnyagin et al. 2007b; Portnyagin and Manea 2008). Beneath the volcanic front, the slab dip angle variations result in slab depths of ~100–140 km, whereas for the CKD volcanoes, depths range from 140 to 180 km in the south to ~100 km below Shiveluch, the northernmost active volcano with slab-melt signatures (Yogodzinski et al. 2001). Shiveluch is located on the westward extension of the transform fault of the Western Aleutians, which abruptly truncates the Kurile–Kamchatka subduction zone (Fig. 1).

Klyuchevskoy and volcanoes of the Central Kamchatka depression

The CKD contains a dozen volcanoes, with the largest cluster found at the Klyuchevskoy group. Modern stratovolcanoes of the group are all less than 50,000 years old and overlie a thick base of mid to late Pleistocene plateau basalts and shield volcanoes (Melekestsev 1980). Klyuchevskoy (Figs. 2, 3) is built upon the flanks of the extinct basalt–andesite volcanoes of Kamen' and Plosky Blizhny (or Krestovsky), and all these volcanoes are underlain with Pleistocene plateau basalts. The pre-Pleistocene basement under the CKD is a mafic intra-oceanic accretionary terrain (Konstantinovskaia 2001).

Klyuchevskoy is the most volcanically active of the group (Figs. 2, 3) and possibly is the most active arc volcano on earth, yielding biannual volcanic eruptions. Its 4,750 m high edifice consists of basaltic to basaltic–andesitic tephra and lavas, and ^{14}C ages suggest that the entire edifice has formed during the last ~7,000 years. Cinder cones started to form on the flanks of the volcano at ~3500 BP (Braitseva et al. 1995).

Seismic tomographic P-wave imaging of the Klyuchevskoy group area shows a significant narrow P-wave anomaly from 20 km depth, which broadens at 30–40 km below the edifice (Piyp and Yefimova 1993; Lees et al.

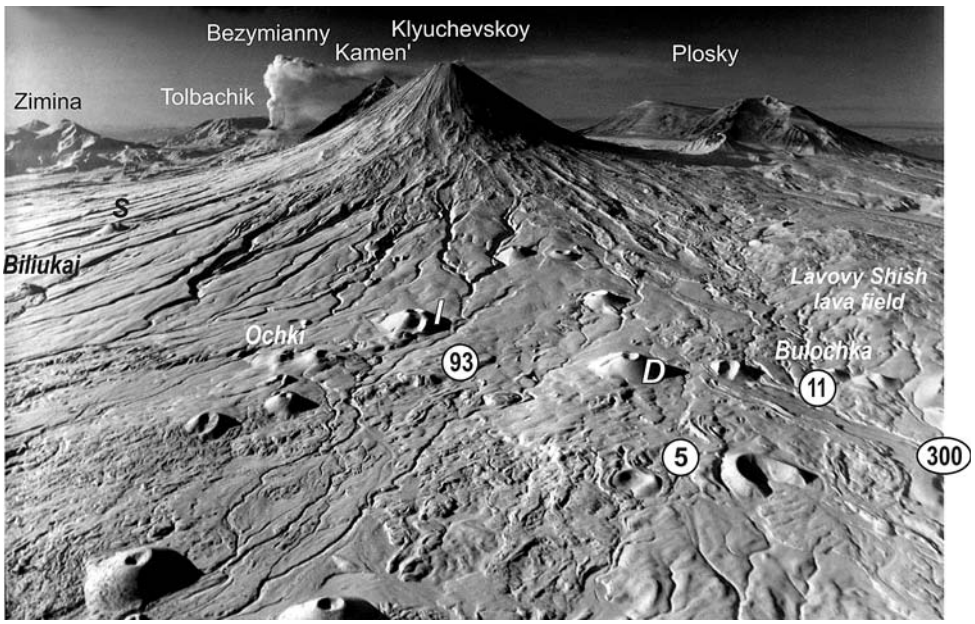

Fig. 2 Klyuchevskoy volcanic group from the northeast. Names of large stratovolcanoes are on the top; two cones of Plosky volcanic massif are Plosky Blizhny (at the foreground, sometimes referred to as Krestovsky) and Plosky Dalny (or Ushkovsky). Bezymianny volcano is erupting on the background. Some of the Klyuchevskoy flank cones mentioned in the text and well seen on the photo are labeled (*S* Biliukai, *I* Ochki, *D* Bulochka). Early Holocene Lavovy Shish lava field differs in composition from Klyuchevskoy rocks and belongs to Plosky volcano. Location of the sampled tephra sections is shown with *white numbered circles*; some site numbers are abbreviated: 93 = 84093, 5 = 05-KLV-5, and 11 = 05-KLV-11. Photo by Vasilii Podtabachnyi

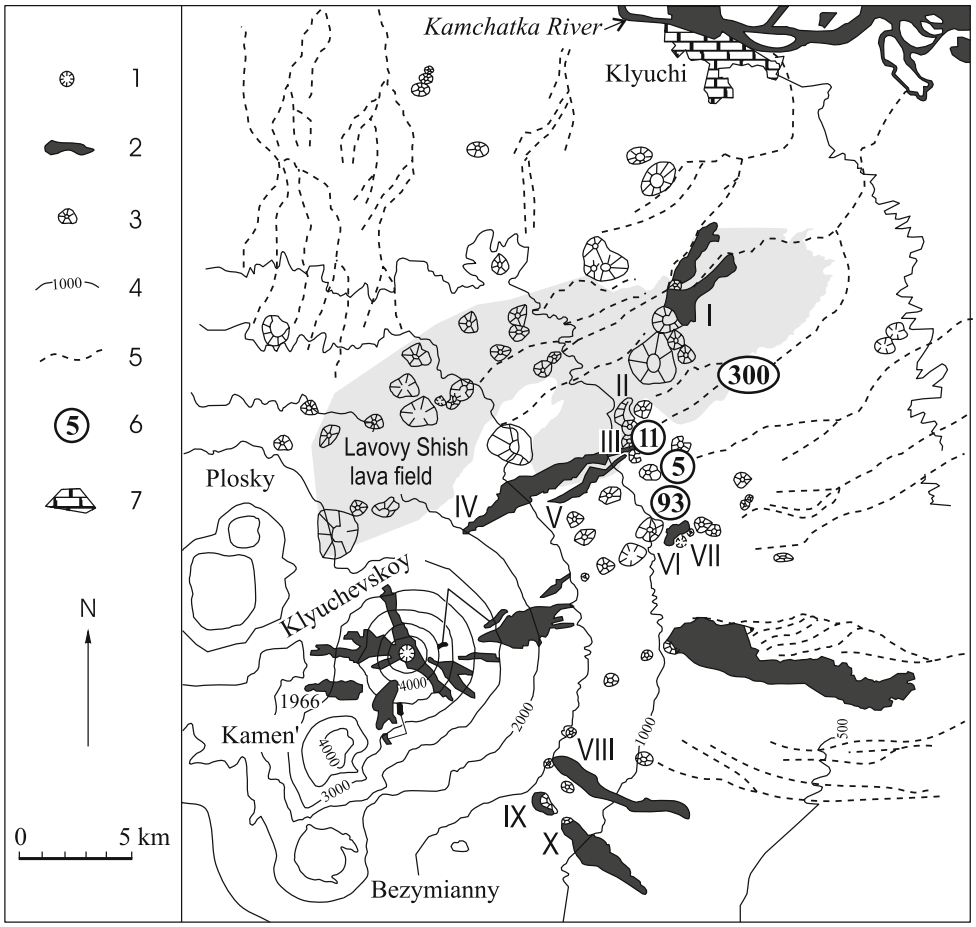

Fig. 3 Location of sampled tephra sections and lava flows. *1* Klyuchevskoy summit crater; *2* Klyuchevskoy historic lava flows; *3* Klyuchevskoy and Plosky flank cinder cones; *4* Contours (elevated in m); *5* dry river valleys; *6* tephra sections (*numbers* as in Fig. 2); *7* Kliuchi town. Sampled lava flows include: *I* Tuyla (1932 AD); *II* Luchitsky; *III* Bulochka; *IV* Piip (1966 AD); *V* Belyankin (1953); *VI* Bylinkina (1951); *VII* Ochki; *VIII* Apakhonchich (1946); *IX* Vernadsky (1956); *X* Zavaritsky (1945). *Light gray area* shows early Holocene Lavovy Shish lava field related to Plosky volcano activity. See Appendix for exact locations and Fig. 5 for stratigraphy of sampled rocks. Map adapted from Ozerov et al. (1997)

2007). These and other researchers infer this conical zone to be the primary magma source for the entire Klyuchevskoy group, with narrow conduits emanating from this source to smaller, secondary magma chambers for each individual volcano.

Chemical and isotopic overview of Klyuchevskoy volcano

The edifice of Klyuchevskoy volcano (Figs. 2, 3) is made of medium-K, high-Mg to high-Al, basaltic andesite (more abundant) and basalt, with olivine, pyroxene, and plagioclase as phenocrysts. Eruptive products more differentiated than basaltic andesite are not found at Klyuchevskoy but are abundant at neighboring Bezymianny volcano (Figs. 2, 3), which erupted andesite and dacite with pyroxene-plagioclase and amphibole-plagioclase assemblages (e.g., Kersting and Arculus 1994; Bindeman et al. 2004). Other volcanoes of the CKD are largely basaltic and span wider compositional ranges from medium- to high-K, high-Al and high-Mg, series (e.g., Volynets 1994; Ozerov 2000; Churikova et al. 2001; Portnyagin et al. 2007b). Bezymianny andesites share common O, Sr, Pb, and Nd isotopic characteristics with Klyuchevskoy (Bindeman et al. 2004; Almeev et al. 2003), and thus are likely derived from Klyuchevskoy-type basalts (e.g., Ozerov et al. 1997).

Klyuchevskoy basalts and basaltic andesites have been studied for several decades, resulting in the creation of several major and trace elemental databases (Appendix A; see also GEOROC website). However, nearly all of the published analyses represent sampling of the same 10–20 historic to <200 BP lavas and scoria cones and repeated analyses of "prehistoric" Bulochka cone, the most magnesium, olivine-rich lava at Klyuchevskoy in the 2200–2700 BP range. An interesting aspect of Klyuchevskoy compositions not commented in previous studies is their subtly elevated SiO_2 content by $\sim$1 wt% for given MgO content (Appendix A). When primitive (Mg#, i.e. Mg/Mg + Fe^{2+}) molar > 0.65 or more evolved (e.g., normalized at MgO = 6 wt%) CKD are compared. Klyuchevskoy rocks have compositions intermediate between basaltic Tolbachik volcano in the south and Sheveluch volcano in the north, the latter having the most silica-rich "adakitic

flavor". Portnyagin et al. (2007b) and Portnyagin and Manea (2008) interpreted the compositional peculiarity of Klyuchevskoy rocks to reflect either relatively low equilibration temperatures of parental Klyuchevskoy melts with mantle peridotite or mixing of primitive basalts with evolved silica-rich melts in shallow conduits or magma chamber.

Perhaps the most intriguing aspect of Klyuchevskoy, Bezymianny, and CKD volcanism in general are the unusually high-$\delta^{18}O$ values of basalts, the highest in the world. Kersting (1991), Pineau et al. (1999), and Pokrovsky and Volynets (1999) reported $\delta^{18}O$ whole-rock values of 5.5–8.5‰, which range from normal mantle-derived basalt values of 5.7‰ (e.g., Eiler 2001) to up to 3‰ higher. Dorendorf et al. (2000), using the laser fluorination technique, reported olivine values from Klyuchevskoy lavas of 5.8–7.1‰ (0.4–2‰ higher than mantle-derived olivine). Comparably high-$\delta^{18}O$ values (with Klyuchevskoy as the extreme) characterize olivine-bearing basalts from all other volcanoes in the CKD (Bindeman et al. 2004; Portnyagin et al. 2007b).

Klyuchevskoy and other volcanoes of the CKD are not alone in producing high-$\delta^{18}O$ basaltic magmas. In our parallel study of another large volcano—Mount Shasta, in the Cascade arc, northern California—we have also found olivine with high $\delta^{18}O$ values of up to 6.2‰ in basalts and basaltic andesites (E. Martin et al., in prep). Like Klyuchevskoy, Mt Shasta is a very active arc volcano, built on over accreted ultramafic terrains in a subduction zone setting, and produces magmas that are H_2O-rich (Anderson 1973; Grove et al. 2006).

Goals of this study and methodology

Motivation for this study stems from an effort to understand the origin of voluminous high-$\delta^{18}O$ basaltic volcanism, the number of localities of which is increasing. Our evidence presented below indicates that mafic magmas at Klyuchevskoy have both high $\delta^{18}O$ and high H_2O concentrations, and we investigate the origin of these distinctive features using a diverse set of tools. We base our study on rapidly quenched tephra from tephrochronologically-defined layers spanning the entire history of Klyuchevskoy. We present oxygen isotope analyses of olivine and matrix glass from these tephra. The olivine-hosted melt inclusion analyses provide H_2O and CO_2 concentrations and estimates of crystallization depths that reveal features of the plumbing system and crystallization processes beneath the volcano. Major and trace element analyses of bulk tephra, lava, and olivine phenocrysts, and ion microprobe analysis of olivine-hosted melt inclusions are examined for geochemical signatures of temporal magma evolution patterns.

Sampling and analytical methods

Sampling of Klyuchevskoy tephra and lava

Lavas available for sampling at lower altitudes on Klyuchevskoy's slopes erupted primarily from flank vents and thus cover only the most recent ~3,500 years of activity. Lavas erupted from the summit crater are covered with thick pyroclastic, landslide and lahar deposits and are exposed only in the chutes high on the edifice (Ponomareva et al. 2006). Locations of lava flows and cinder cones sampled for this study are shown in Fig. 3. In contrast to previous petrologic and geochemical studies, we focused primarily on Klyuchevskoy tephra. Advantages of tephra studies include complete coverage of the eruptive history, age control of the samples using dated marker ash layers (Fig. 4, Braitseva et al. 1997), and good preservation of melt inclusions due to rapid quenching of tephra. Figure 5 shows the stratigraphy of the sections we sampled and the marker beds that were used for tephrochronology. Tephra samples for this

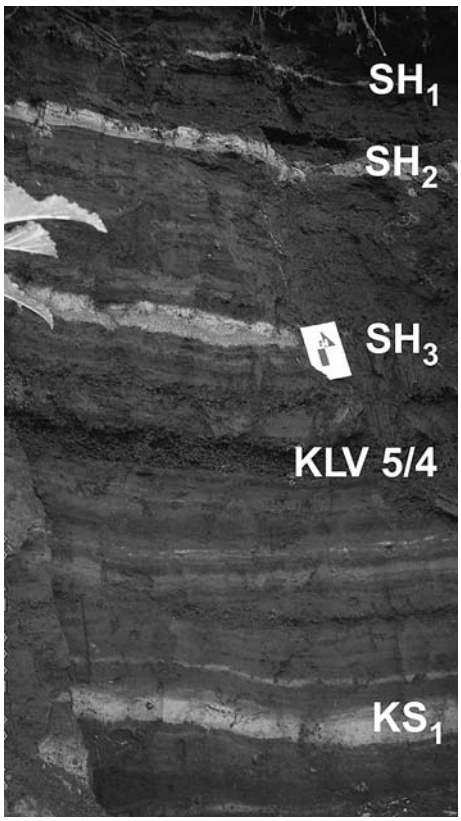

Fig. 4 A fragment of soil-pyroclastic sequence at the Klyuchevskoy slope. Klyuchevskoy cinders are interlayered with thin sandy loams and marker tephra beds. Marker tephra layers: SH_1 (^{14}C age 250 y BP), SH_2 (950 yr BP), and SH_3 (1400 yr BP) from Shiveluch volcano; KS_1 (1800 yr BP) from Ksudach volcano. Codes and ages of marker tephra layers according to Braitseva et al. (1997). KLV-5/4, sample of Klyuchevskoy cinders

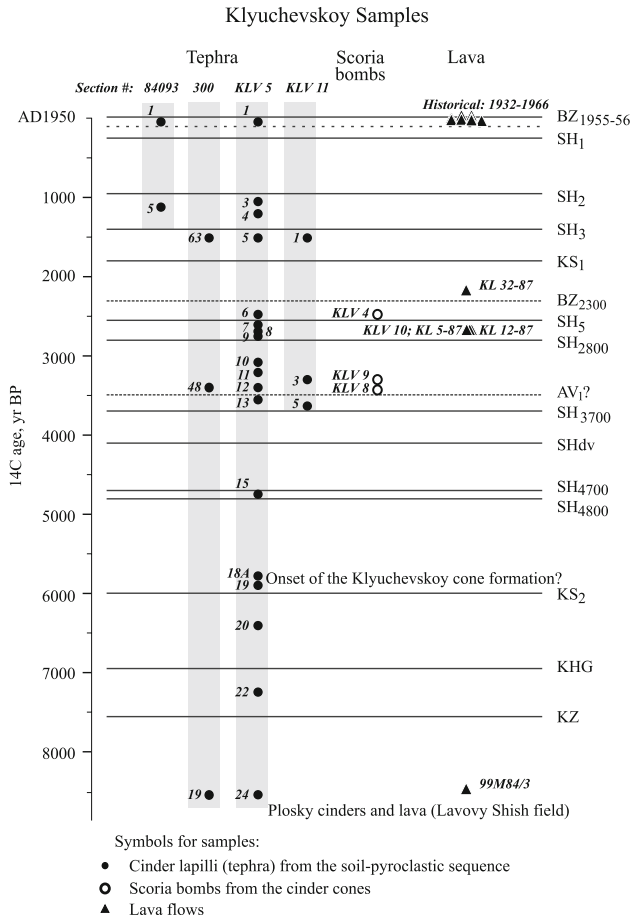

Fig. 5 Stratigraphic position of sampled eruptive products. Most of the samples, except for the three oldest ones, represent Klyuchevskoy activity. The age of Klyuchevskoy cone was previously estimated at ~5.9 ka (^{14}C) based on presence of a widespread thick package of stratified cinders (our section KLV-5, samples 18A and 19), which were thought to represent Klyuchevskoy initial cone-building eruptions (Braitseva et al. 1995). Two older samples (KLV-5/20 and 22), however, are very similar to other Klyuchevskoy products (Supplementary Table 1) indicating that minor eruptions of similar magma took place earlier. Three oldest samples (300/19, KLV-5/24, and 99M84/3) dramatically differ from Klyuchevskoy rocks and represent early Holocene Plosky volcano activity (a number of cinder tephras probably from a summit caldera, cinder cones, and Lavovy Shish lava field) predating Klyuchevskoy. These oldest sampled Holocene products overlye glacial till and late Pleistocene lava (sample KLV-38, not shown). Widespread, radiocarbon dated Holocene tephra marker beds from explosive Kamchatkan eruptions are shown with *horizontal lines* and labeled at the *right*. *SH* tephras from Shiveluch volcano, *BZ* Bezymianny, *KS* Ksudach, *AV* Avachinsky, *KHG* Khangar, *KZ* Kizimen. Codes and ages of marker tephra beds according to Braitseva et al. (1997) and Ponomareva et al. (2007). These marker beds were used to determine the age interval of studied eruptive products

study come from several riverbank outcrops around the NE quadrangle of Klyuchevskoy volcano (Figs. 2, 3) and include the nearly entire Holocene record of mafic explosive volcanism in the area. In this work we sampled only tephra layers thicker than 5 cm, with lapilli ≥1 mm, and which exhibited no sorting by water. Sand sized and smaller particles were not analyzed due to the possibility of aeolian segregation and mixing of multiple deposits.

Analytical methods

Selected samples were analyzed by several methods: oxygen isotopes of individual and bulk phenocrysts of olivines and host glass by CO_2 laser fluorination, water and CO_2 concentrations of doubly-polished melt inclusions in olivines by FTIR, electron microprobe and ion microprobe analyses of melt inclusions, and by whole-rock analysis of samples. Details of analytical procedures can be found in electronic supplement to this paper.

Results

Lava and tephra record of Klyuchevskoy volcano: high-δ^{18}O, high-Al and normal to high-δ^{18}O, high-Mg basalt

Our investigation of tephra layers pushed back the age of onset of Klyuchevskoy activity by ~1.5 kyr. The age of Klyuchevskoy's edifice was previously estimated at ~5.9 ka (^{14}C) based on the presence of a widespread, thick package of stratified tephra (our section KLV-5, samples 18A and 19) that were thought to represent the initial cone-building eruptions (Braitseva et al. 1995). Two older samples (KLV-5/20 and 22) that we studied, however, are geochemically very similar to other Klyuchevskoy products (Supplementary Table 1), indicating that minor eruptions of similar magma took place 1.5 kyr. earlier. Our data do not confirm the suggestion of Ariskin et al. (1995) that high-Mg basalts erupted earlier in the history of Klyuchevskoy and that later magmas were more differentiated (predominantly high-Al compositions). For example, 2200–2700 BP Bulochka high-Mg basalts, once considered to be parental to the subsequent eruptions, were preceded by lower-Mg basalts (Supplementary Table 1).

Our whole-rock MgO and Al_2O_3 data for tephra spanning the entire history of Klyuchevskoy show a continuous range between high-Mg (7–12.5 wt% MgO), and high-Al (17–19 wt% Al_2O_3, 3–6.5 wt% MgO) basalts, with olivine-rich cumulate lavas (11–12.5 wt% MgO) forming a separate cluster (Fig. 6, Appendix A). These data overlap with previously published analyses of recent lavas (Fig. 6). We have plotted histograms (Fig. 7) of all published analyses of Klyuchevskoy rocks from the GEOROC database in addition to recently published data from Portnyagin et al. (2007a,2007b) and data from this study. Whereas the majority of our tephra samples are high-Al, we find three maxima on the MgO and Al_2O_3 histograms. Two maxima

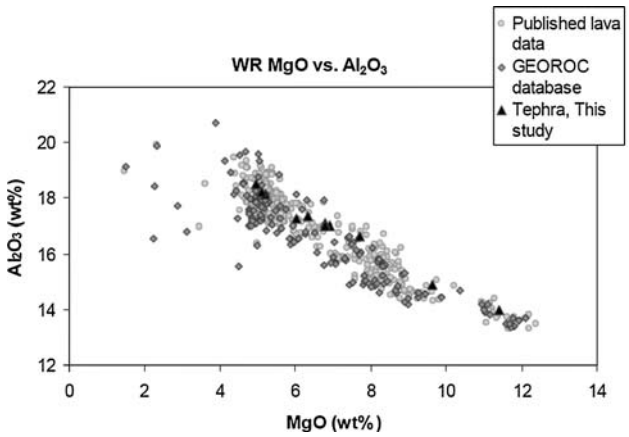

Fig. 6 Compositional variations of MgO and Al_2O_3 within collected lava samples and tephra (this study) throughout the eruptive history of Klyuchevskoy. There is a negative correlation between MgO and Al_2O_3 and an overlap between tephra analyses presented here and published data (Portnyagin et al. 2007a, 2007b, GEOROC data is from http://georoc.mpch-mainz.gwdg.de/georoc/Entry.html)

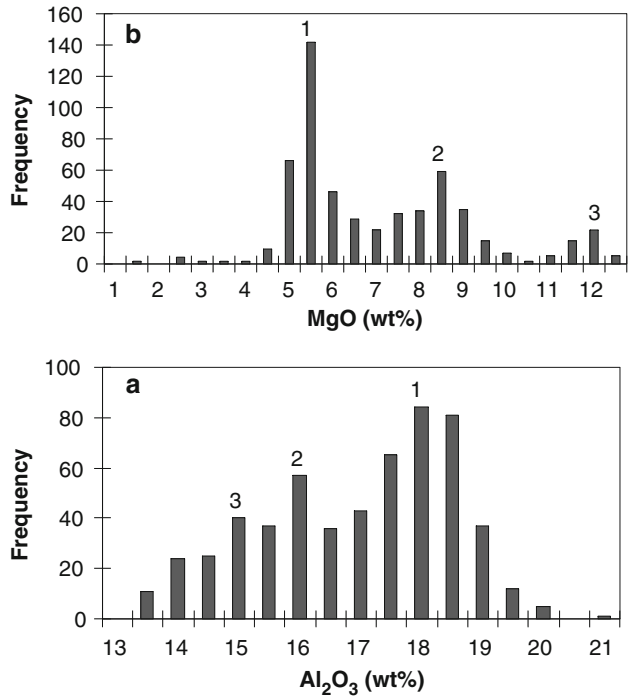

Fig. 7 Frequency of Klyuchevskoy whole-rock compositions for **a** MgO and **b** Al_2O_3. Data are from this study and compiled from the GEOROC database and Portnyagin et al. (2007a, 2007b). Three peaks mark high-Mg, intermediate, and high-Al groups, discussed in text

correspond to the above-defined high-Mg and high-Al compositional groups based on tephra, and the third maximum relates to the group of samples with the highest MgO. This group, represented by crystal-rich Bulochka cone basalts, has likely formed due to olivine accumulation.

When plotted against age, we see a wave-like evolutionary trend throughout Klyuchevskoy's history with intermittent periods of activity yielding high-MgO, high-Al_2O_3, or high-$\delta^{18}O$ vs. more normal-$\delta^{18}O$ magmas (Appendix A, Fig. 8). In fact, coeval eruption of both high-Al and high-Mg basalts occurred together in some eruptions (e.g., 1951 AD Bylinkinoi cone, 1938 AD Bilyukai, and Tuila 1932 AD; e.g., Khubunaya et al. 2007).

Nearly all of the samples from each of the different compositional groups are enriched in $\delta^{18}O$ with respect to mantle values, with high-Al to intermediate basalt being the most enriched (7.7–8.1‰ for groundmass glass), with values that are >2‰ higher than mantle melts (Table 1). The $\delta^{18}O$ values of groundmass in tephra and lava samples show a trend of increasing $\delta^{18}O$ with increasing whole-rock Al_2O_3 and decreasing MgO (Fig. 9). However, fractional crystallization of a high-Mg basaltic parent to form a more evolved high-Al basalt cannot explain the ~1‰ higher $\delta^{18}O$ values of high-Al basalts compared to the high-Mg basalts (e.g., Bindeman et al. 2004), ruling out the possibility of a simple fractional crystallization relation between the two types. Bulk and individual olivine analyses in these samples exhibit considerable scatter around the overall trends, yielding low R^2-values for plotted trendlines (Fig. 10). The scatter in the $\delta^{18}O$ olivine values is explained by magma mixing and olivine recycling, as discussed below.

Analyses of megaplagiophyric tephra that predate the modern Klyuchevskoy cone, as well as analyses of Bezymianny volcano (Bindeman et al. 2004) and neighboring volcanoes in the CKD (Portnyagin et al. 2007b), demonstrate that the high-$\delta^{18}O$ signature extends deeper into time record and is also extensive laterally. Our interpretations for Klyuchevskoy may therefore be relevant for understanding the origin of other high-$\delta^{18}O$ and (potentially H_2O-rich) magmas in the CKD and beyond.

$\delta^{18}O$ evidence for olivine recycling

Individual olivines analyzed in this study show evidence for oxygen isotope disequilibrium with their host glasses (Fig. 10). However, the extent of disequilibria and heterogeneity of olivine $\delta^{18}O$ varies from sample to sample, and some samples have olivines with a wide range of $\delta^{18}O$, showing as much as 1‰ deviation from equilibrium values. To assess isotopic equilibrium or disequilibrium between olivines and their host groundmass glass (Fig. 10), olivine-melt fractionation factors need to be determined. We followed the procedure of Eiler (2001) and Bindeman et al. (2004), which involves recalculation of melt composition into normative mineral components. For each of the normative mineral components, we used the corresponding experimental mineral-olivine isotope fractionation

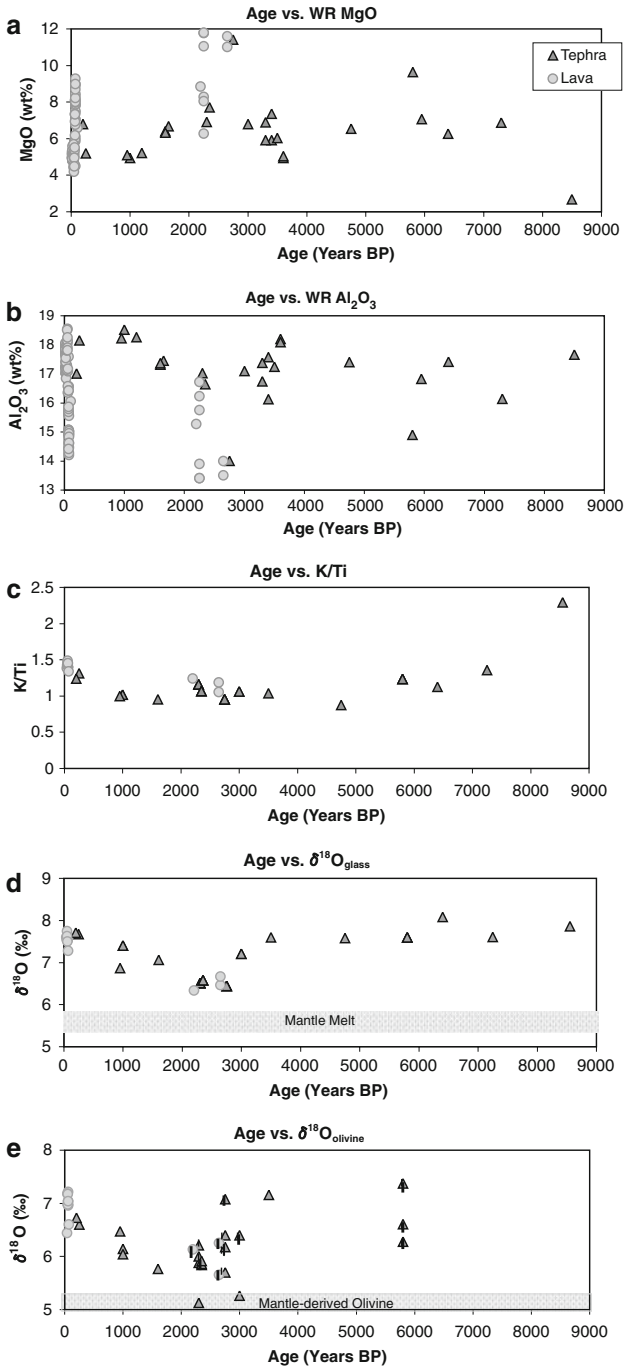

Fig. 8 Compositional and isotopic variations against age. **a** MgO; **b** Al_2O_3; **c** K/Ti; **d** $\delta^{18}O_{glass}$; **e** $\delta^{18}O_{olivine}$. This diagram plots tephra samples vs. previously published lava samples (see Figs. 6, 7). Wave-like evolutionary trends are evident and analyses of tephra and lava overlap. This suggests coeval eruption and mixing of high-Al, high-Mg, and high-$\delta^{18}O$ and low-$\delta^{18}O$ basalts, tephra or lavas in geologic record of Klyuchevskoy volcano. All plotted oxygen isotope analyses for tephras and lavas in (**d, e**) were performed in the University of Oregon stable isotope lab, *vertical line* inside some *symbols* in (**e**) marks single crystal olivine oxygen isotope analyses marked as ol-1 in Table 1

coefficients of Chiba et al. (1989). These coefficients were then used to calculate the isotope equilibrium between melt (sum of all normative mineral components) and olivine using the following equation: $1{,}000\ \ln\alpha_{melt\text{-}olivine} = \Delta^{18}O_{melt\text{-}olivine} = (A{\cdot}W{\cdot}10^6T^{-2})$; where T is the estimated temperature of crystallization, W is the weight fraction of each normative mineral component in the melt, and the sum of all the W's is equal to 1. For the calculations, we estimated crystallization temperatures in the range of 1,100–1,250°C using the MELTS program (Ghiorso and Sack 1995). Calculated equilibrium melt-olivine isotope fractionation for high-Mg samples (~1,140°C) was ~0.7‰, whereas high-Al and intermediate composition samples at the same temperature yielded values of ~0.8‰. If the high-Al basalts crystallized olivine at ~40°C lower than the high-Mg samples, the $\Delta^{18}O_{melt\text{-}olivine}$ value is ~0.85‰.

Measured $\delta^{18}O_{olivine}$ values in each studied sample are compared with calculated equilibrium $\delta^{18}O$ values in Fig. 10. A remarkable observation is that individual olivine in most samples, lava or tephra, are characterized by dis-equilibrium olivine–groundmass relationships. In every sample, olivines range from being in isotopic equilibrium to being up to 1.2‰ lighter to 1.5‰ heavier than the equilibrium value.

We discount the possibility of secondary $\delta^{18}O$ modification of tephra clasts due to post-depositional alteration because the tephra deposits are very young (<7,000 years old), optically fresh, and contain little or no absorbed water in XRF analyses (<1 wt%). Even more hydrous samples with 1–2.7 wt% water reproduced $\delta^{18}O$ values with better than ±0.11‰. The $\Delta^{18}O_{melt\text{-}olivine}$ disequilibria is also present in historic lava samples where glass is dense and less vesicular. It is quite possible however, that pre- to syneruptive modification of $\delta^{18}O$ value of magma (by less than 1‰) was caused by interaction with low-$\delta^{18}O$ hydrothermally-altered rocks in the Klyuchevskoy edifice as is observed in Iceland (Bindeman et al. 2006) and Hawaii (Garcia et al. 1998), but widespread high- (not low-) $\delta^{18}O$ values of matrix glass suggest that this process was limited. Therefore, this range of isotopic disequilibrium is interpreted to be largely due to recycling of variable-$\delta^{18}O$ olivine cumulates, that are also in compositional Fe–Mg disequilibrium with their host magma.

Fe–Mg disequilibrium between olivine and melt

Electron microprobe analyses of olivines and their host groundmass glass (re-melted using the laser as described in Sect. "Sampling and analytical methods") were used to check for compositional Fe–Mg equilibrium (Fig. 11) in

Table 1 Oxygen isotope analyses on individual and bulk phenocrysts and groundmass glass from Klyuchevskoy volcano

Tephra section no.	Sample no.	Material	Source	^{14}C age, year BP	Mineral type	δ^{18}O olivine	δ^{18}O glass	Std Error (*n*) glass
84093	1	Cinder lapilli		200	Ol	6.73	7.71	0.12 (2)
“ “	5	“ “		1150	Ol	6.47	6.60	0.08 (4)
								5.83, 6.00
–	KLV 4	Scoria bombs	Cone D	2500	Ol-1	6.21		
					Ol	5.88		
					Ol-1	6.00		
					Ol-1	5.13	6.51	0.15 (6)
KLV 5	1	Cinder lapilli		50	Ol	6.60	7.68	0.02 (2)
“ “	3	“ “		1100	Ol	6.15		
					Ol	6.04	7.40	0.11 (2)
“ “	4	“ “		1200	Ol	7.62	7.38	0.11 (5)
“ “	6	“ “	Cone D	2500	Ol-1	5.84		
					Ol-1	5.86		
					Ol-1	5.92	6.58	0.07 (2)
“ “	7	“ “		2600	Ol	5.76		
“ “	8	“ “	Bulochka cone?	2650	Ol-1	6.18		
					Ol-1	6.40		
					Ol-1	7.08		
					Ol-1	5.70	6.44	0.11 (6)
“ “	9	“ “		2700	Ol	6.09		
					Ol-1	5.52		
“ “	10	“ “		3000	Ol-1	6.40		
					Ol-7	5.26	7.21	0.05 (2)
“ “	11	“ “		3100	Ol-2	6.26		
					Ol-2	6.19	7.06	0.04 (2)
“ “	15	“ “		4750			7.58	0.09 (2)
“ “	18a	“ “		5700	Ol-1	6.27	7.53	0.12 (5)
					Ol-1	6.61		
					Ol-1	7.37		
	20	“ “		6400			8.08	0.01 (2)
	22	“ “		7250			7.61	0.14 (2)
	24	“ “	Plosky	8550			7.86	0.07 (2)
300	19	“ “	Plosky	8550	Plag-1	7.40		
	48	“ “		3500	Ol	7.16	7.60	0.13 (2)
	63	“ “		1600	Ol	5.77	6.93	0.13 (3)
–	KL 32-87	Lava	Ochki cone	2200	Ol	6.13	6.36	0.03 (3)
					Ol	6.36		
–	KL 5-87	“ “	Bulochka cone	2650	Ol	6.25	6.40	0.12 (3)
					Ol	6.03		
–	KLV 10	“ “	“ “	2650			6.58	0.14 (2)
–	KL 12-87	“ “	Luchitsky cone	2650	Ol	5.65	6.66	0.06 (2)
–	99M-84/3	“ “	Lavovy Shish	8500	Plag-1	7.37		
–	KL 45-87	“ “	Tuyla cones	AD 1932	Ol	6.13	7.28	0.01 (2)
					Ol	6.94		
	Zav 50-49	“ “	Zavaritsky cone	AD 1945	Ol-1	7.04	7.49	0.00 (2)

Table 1 continued

Tephra section no.	Sample no.	Material	Source	^{14}C age, year BP	Mineral type	δ^{18}O olivine	δ^{18}O glass	Std Error (*n*) glass
–	AP 60-31	“ “	Apakhonchich cone	AD 1946	Ol	7.21	7.47	0.07 (3)
					Ol-1	7.04		
					Ol	6.96		
					Ol	6.98		
–	Byl 69-38	“ “	Bylinkina cone	AD 1951	Ol	6.98	7.74	0.01 (2)
					Ol	6.98		
–	Bel 70-46	“ “	Belyankin cone	AD 1953	Ol	7.17	7.62	0.01 (2)
					Ol	7.13		
–	V68-37	“ “	Vernadsky cone	AD 1956	Ol	7.18	7.51	0.05 (3)
					Ol	7.07		
–	KLV 6	“ “	Piip cone	AD 1966			7.09	0.16 (3)
–	Piip 79-50	“ “	“ “	“ “	Ol	6.44	7.60	0.02 (2)
	KLV 38		Plateau basalt	Late Pleistocene	Plag-1	6.62		

Italicized values were not used in Std Error calculations as they were extreme outliers. Tephra layers originated either from flank cones or from summit crater, exact sources for most of them cannot be identified. See Appendices A and B, and Figs. 3 and 5 for sample localities, stratigraphic positions and chemical compositions

Ol is bulk olivine analysis, *Ol-#* indicates number of olivine per analysis

selected high-Al and high-Mg samples of tephra from which we also analyzed melt inclusions. The wide range of olivine Mg#'s within individual samples of intermediate composition clearly indicate the lack of equilibrium between many olivine crystals and their host glass. In contrast, high-Mg and high-Al samples contain olivines that are mostly in Fe–Mg equilibrium with their host glasses, and the olivines show little zoning.

Similar to the approach here, equilibrium K_D calculations were done previously by Kersting and Arculus (1994) with olivine and augite from high-Mg and high-Al basalts. They determined that high-Mg basalts were in equilibrium with Fo_{90} olivine, and thus represent primitive mantle melts, whereas high-Al basalts were in equilibrium with more Fe-rich olivine. Intermediate compositions were characterized by complex disequilibrium zoning patterns. Khubunaya et al. (2007) reported even more complex olivine zoning patterns and wide Fo ranges within many historic lavas, including both high-Al and high-Mg types, and found maximum olivine Fo content of 91.4. Furthermore, most Mg-rich lavas, including Bulochka, the most Mg-rich basalt in Klyuchevskoy, exhibit a bimodal or even trimodal distribution of Fo in cores of olivines with maxima at 91.4–87, 85–83, and <80. Khubunaya et al. (2007) concluded that the most forsteritic olivines found in Klyuchevskoy high-Mg basalts represent xenocrysts from cumulates of more primitive magma rather than being from disintegrated mantle peridotitic nodules.

These results from previous studies are consistent with our new data, with the exception that our high-Al samples have olivines that are closer to equilibrium with their host glasses. However, both our new data and the published data support the idea of magma mixing and olivine recycling between high-Al and high-Mg basaltic magmas.

Melt inclusion volatile concentrations

We analyzed H_2O and CO_2 in olivine-hosted melt inclusions from six tephra samples spanning the compositional and δ^{18}O range at Klyuchevskoy. (Figs. 12, 13). The highest H_2O values of 7.1 and 5.3 wt% were found in Fo_{80} olivine in the most Al-rich sample (300-5/63) (Fig. 12, Supplementary Table 2). The highest CO_2 concentration of 1,884 ppm was found in sample KLV 5/18a, with a corresponding H_2O value of 4.2 wt% (Fig. 13). The lowest values were $\sim$1 wt% H_2O, and many samples contained CO_2 below the detection limit of $\sim$50 ppm. This wide range of CO_2 and H_2O values is likely caused by degassing and olivine crystallization during magma ascent, but the nature of the degassing processes that can create such variations is still poorly understood and likely involves open system processes (e.g., Spilliaert et al. 2006; Johnson et al. 2008). The highest volatile concentrations, therefore, are our best estimate of original magmatic concentrations. Vapor saturation pressures calculated for these volatile contents (using the VolatileCalc program; Newman and

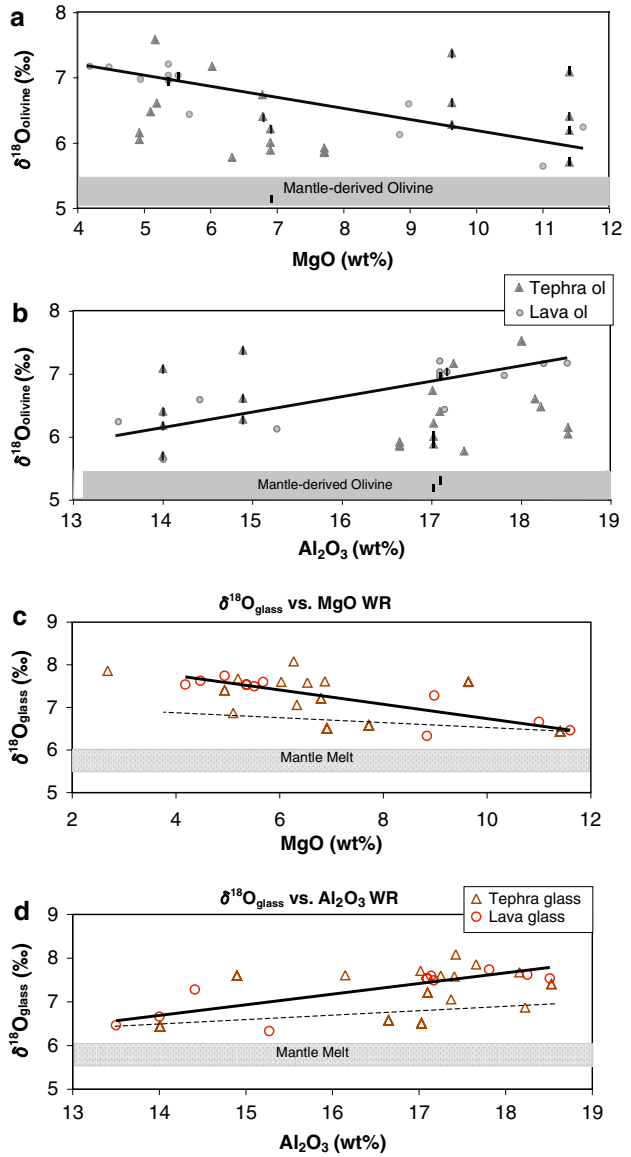

Fig. 9 $\delta^{18}O$ for glass, olivine vs. MgO and Al_2O_3. Both high-Al and high-Mg basalts and their olivines are significantly higher in $\delta^{18}O$ than the mantle, with high-Mg basalts being ~1‰ higher, and high-Al being ~2‰ higher. Notice, a negative correlation is present for (**a, c**) $\delta^{18}O_{olivine}$ and $\delta^{18}O_{glass}$ vs. MgO and a positive correlation of oxygen isotope parameters with Al_2O_3 (**b, d**). High-Al basalt cannot be a result of fractional crystallization of a single parental moderately high-$\delta^{18}O$, high-Mg basalt (see *dashed fractionation line* and text for explanation). Individual olivine phenocrysts (*vertical line* in selected samples) exhibit large $\delta^{18}O$ range in many samples; other olivine analysis (*symbols with no vertical line*) reflect analysis of typically two to three grains that can cause some averaging of these diverse individual $\delta^{18}O_{olivine}$ analysis. This large $\delta^{18}O_{olivine}$ range is likely due to olivine recycling through magma mixing and cumulate addition. These high-Mg and high-Al basalts have erupted coevally throughout the history of Klyuchevskoy (see Fig. 8)

Lowenstern 2002) indicate a maximum depth of crystallization of ~17 km (5 kbar) for melts with 1,884 ppm CO_2 and 4.2 wt% H_2O.

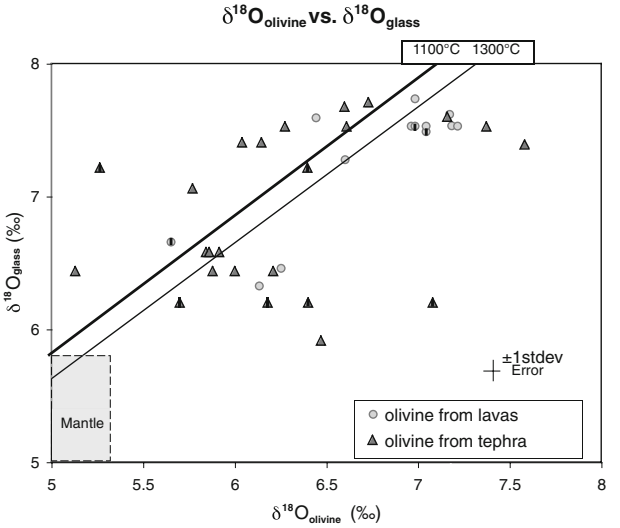

Fig. 10 $\delta^{18}O_{olivine}$ vs. $\delta^{18}O_{glass}$ diagram displaying that olivines in single sample span significant $\delta^{18}O$ ranges and many are out of equilibrium with the groundmass. Black lines represent calculated $\Delta^{18}O_{melt\text{-}olivine}$ oxygen isotope fractionation at indicated temperatures using CIPW norms of melt and fractionation factors from Chiba et al. (1989), see text for further discussion

We have obtained the highest reported H_2O concentrations for Klyuchevskoy for high-Al basalts, with many values between 3.0 and 5.3 wt% and extending to as high as 7.1 wt%; these values are among the highest reported for arc basaltic magmas. Gurenko et al. (2005) measured up to 5.5–6.4 wt% water in olivines from the basaltic Chikurachki volcanoes in northern Kurile Islands. Other arc basalts such as those from Cerro Negro (Nicaragua), the Marianas, and the central Trans-Mexican Volcanic Belt, range up to 6 wt% H_2O (Wallace 2005), and high-Mg andesites from Mt Shasta also contain as much as 6.4 wt% H_2O (Anderson 1973; A.T. Anderson, unpublished data). We attribute our discovery of such high H_2O values to our emphasis on tephra samples that were rapidly quenched and thus preserved the high H_2O concentrations. Previous studies of natural or reheated melt inclusions in primitive to moderately evolved olivine ($Fo_{91\text{-}85}$) from Klyuchevskoy lavas and volcanic bombs (e.g., Sobolev and Chaussidon 1996; Mironov et al. 2001; Portnyagin et al. 2007a) obtained lower concentrations of H_2O (<4 wt%) and no detectable CO_2. In our dataset, however, there is no obvious correlation of maximum measured water concentration in melt inclusions and $\delta^{18}O_{olivine}$ values (not shown). This suggests either decoupling of these two parameters during magma generation, or decoupling during magma ascent as a result of degassing before melt inclusion entrapment, olivine recycling, and magma mixing.

Sulfur concentrations in the melt inclusions vary mostly between 1,000 and 2,900 ppm (Supplementary Table 2). These values are within the range reported by Portnyagin

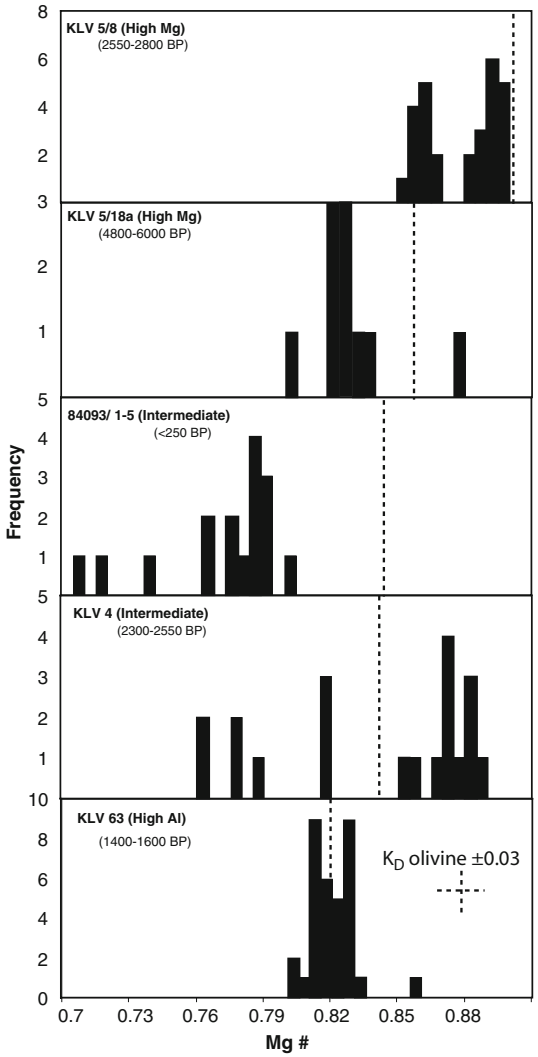

Fig. 11 Olivine–groundmass Mg–Fe equilibrium assessed using electron microprobe data on olivine and melted groundmass. Compositions of olivines that would be in equilibrium with the analyzed groundmass glass in each sample are shown by the *dashed lines*. These equilibrium olivine Mg# values are calculated from measured Mg# of melted groundmass using $K_D = 0.3 \pm 0.03$. Olivine cores in high-Al and high-Mg samples are close to the expected equilibrium with their host glass whereas intermediate samples have mixed populations of olivines, which were likely brought together by magma mixing and/or cumulate entrainment

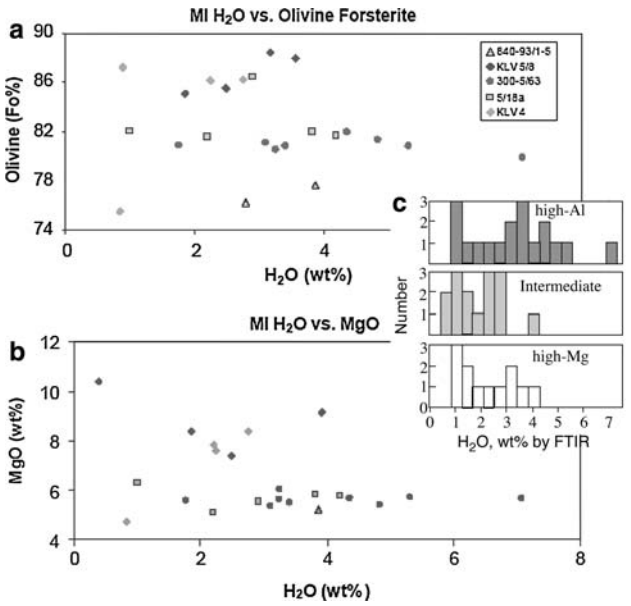

Fig. 12 Water concentrations in melt inclusions vs. compositional parameters **a** forsterite contents of host olivines; **b** MgO of melt inclusions (MI)—corrected for post entrapment crystallization; **c** Histograms of H_2O measured in melt inclusions for all samples. Analyses of melt inclusions and olivines are given in Supplementary Table 2. The highest water contents of 7.1 wt% is measured in Fo_{80} olivine-hosted melt inclusion (high-Al sample 300-5/63), which has olivines in Fe–Mg equilibrium with the host glass. The lowest water concentrations in each sample are likely due to pre-entrapment degassing

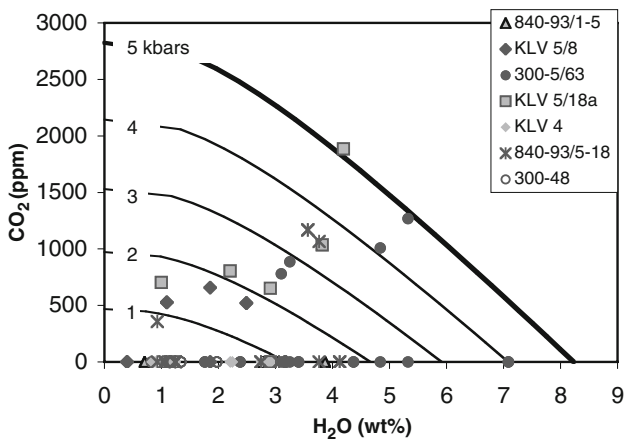

Fig. 13 H_2O vs. CO_2 concentrations in melt inclusions. A wide range of volatile concentrations are present and correspond to partial pressures of 0–5 kbar, as indicated by the vapor saturation isobars (*dark curved lines*; calculated using Newman and Lowenstern 2002). The maximum CO_2 concentration (1,884 ppm with 4.2 wt% H_2O) corresponds to 5 kbar pressure or a maximum depth of crystallization of ~17 km

et al. (2007a) and Churikova et al. (2007) for rehomogenized and glassy melt inclusions from Klyuchevskoy lavas and are similar to values for other mafic subduction related magmas (Wallace 2005; Johnson et al. 2008). Such high values in arc magmas reflect both oxidation (>NNO) and/or addition of S to the mantle wedge by subduction processes (Wallace 2005). Values of S/K_2O in melt inclusions at Klyuchevskoy (S/K_2O = 0.2–0.6) and other CKD volcanoes are higher than that are found either closer to the trench along the volcanic front in Kamchatka or in the back-arc volcanoes (Churikova et al. 2007). Chlorine concentrations in the Klyuchevskoy melt inclusions are mostly between 400 and 950 ppm, but some values range

as high as 1,300 ppm (Supplementary Table 2). The highest Cl values are found in high-Mg sample KLV 5/18a, but otherwise, Cl values are similar in melt inclusions from high-Mg and high-Al samples.

Trace element variations in melt inclusions

Trace element concentrations in melt inclusions measured by SIMS from both high-Mg and high-Al basalts (Supplementary Table 2), when normalized to primitive mantle values (e.g., Sun and McDonough 1989), exhibit a typical pattern for arc basalts (Fig. 14), with depletions in high field strength elements (HFSE) and enrichments in large ion lithophile elements (LILE). Furthermore, melt inclusions in high-Mg and high-Al basalts have trace element patterns that, to a first order, are similar to each other but differ in absolute concentration levels, with the high-Al basalts generally being more enriched. Below we explore whether these differences could be related by fractional crystallization of a parental high-Mg basalt that leads to the enrichment of incompatible trace elements in the high-Al basalts.

Major element crystallization modeling (using the MELTS program) involving fractionation of olivine and clinopyroxene shows that 20% fractional crystallization is required to yield high-Al basalt from end-member compositions of this study involving Fo_{88} to Fo_{80} olivines. This 20% fractional crystallization would produce evolved melts in equilibrium with Fo_{80} olivine if crystallization started from a high-Mg basaltic parent with 9 wt% MgO that initially crystallized Fo_{88} olivine. This estimate of 20% fractionation can be used to recalculate incompatible trace element concentrations in the high-Al basalts to compare primitive melt compositions for both basalt types. The results of this calculation show that there are no significant differences in Ba, U, Sm, Eu, Dy, Y, and Yb between high-Al and high-Mg end members when accounting for the effects of fractional crystallization. However, there are slightly higher concentrations of H_2O, Be, B, and Li in recalculated high-Mg parent for high-Al samples compared to values measured in high-Mg melt inclusions (Fig. 15). These results show that fractional crystallization alone of the high-Mg basaltic magmas cannot account for the chemical characteristics of the high-Al basalts, a conclusion that is consistent with the differences in oxygen isotope ratios. We also note that $^{87}Sr/^{86}Sr$ values of high-Al and high-Mg samples are different, with 0.70366 in high-Al and 0.70355 in high-Mg samples (Dorendorf et al. 2000). We conclude that a different high-Mg basaltic parent with higher $\delta^{18}O$, $^{87}Sr/^{86}Sr$ values and higher H_2O, Be, B, and Li concentrations is a possibility to produce the high-Al basalts through fractional crystallization, though such basalts have not been found by us as whole rocks.

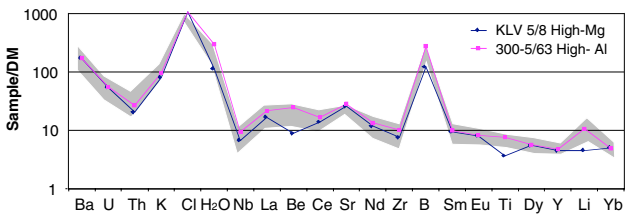

Fig. 14 Spider diagram of trace elements in olivine-hosted melt inclusions within tephra from Klyuchevskoy volcano (see Supplementary Table 2 for analyses). **a** Average composition of high-Mg (KLV 5/8) and high-Al (300-5/63) melt inclusions normalized to a depleted mantle that emphasizes the island-arc, zigzag pattern with peaks in fluid-mobile and depressions in fluid immobile elements

Discussion

We have examined Klyuchevskoy's magmatic history through a variety of techniques, and in the following sections we attempt to interpret this information to better understand the sources and processes involved in magma evolution at this volcano. In particular we evaluate processes that may have caused the observed high $\delta^{18}O$ values and high H_2O contents in Klyuchevskoy magmas and the different trace element and isotopic values of the high-Al and high-Mg basalt types. We then outline differences with previously published models for Klyuchevskoy and CKD volcanism (Dorendorf et al. 2000; Bindeman et al. 2004; Portnyagin et al. 2007b), and present a tectonic context in which hydrous high-$\delta^{18}O$ magmas are formed. We start with a discussion of the high magma production rate and

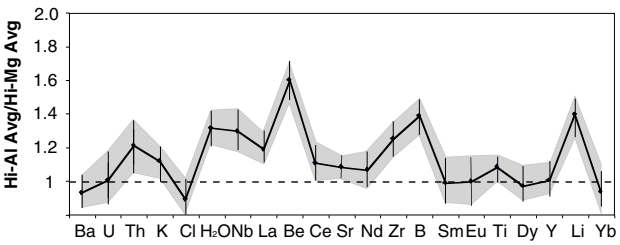

Fig. 15 Trace element comparison of high-Al to high-Mg samples. Average composition of four high-Al melt inclusions in sample 300-5/63 were normalized to the average of three high-Mg melt inclusions in sample KLV 5/8, with high-Al sample 300-5/63, all calculated back to a single Fo_{88} composition, the same Fo as in KLV 5/8, see Supplementary Table 2 for analyses. Elements falling around 1 are found in similar concentrations for both high-Al and high-Mg samples. Elements falling below 1 or above 1 are depleted or enriched in the high-Al sample respectively compared to the high-Mg sample. It appears that H_2O, Li, Be, and B are higher in melt that is parental to high-Al basalt. Water concentrations on this plot represent three highest, least degassed values for high-Al and high-Mg basalts

the complexities of crystal-melt isotopic and chemical disequilibria shown by our data.

High magma production rates

Our results based on tephrochronology suggest that volcanic activity compositionally comparable to Klyuchevskoy started with sample KLV 5/22 (Fig. 5) that shortly postdates the Kizimen (KZ) 7550 BP tephra. Samples between the glacial moraines (dated at ~10,000 BP) and the Kizimen tephra belong to the subalkaline Plosky volcanic system that erupted more differentiated, plagiophyric tephras and lavas with much higher K_2O/Na_2O, K_2O/TiO_2, and total alkali content than any of the Klyuchevskoy cone basalts and basaltic andesites (Fig. 8c). The main stage of Klyuchevskoy cone formation started, however, at ~5.9 ka (^{14}C) (or ~6.8 calibrated ka) based on thick and widespread cinders found at this age interval (Braitseva et al. 1995; samples KLV 5/18A and 19, Fig. 5).

The total volume of Klyuchevskoy's cone is estimated to be 270 km^3 or 0.6×10^{12} tons (Melekestsev 1980), and thus the average magma output rate is estimated to be 0.04 km^3/year (0.09×10^9 tons/year) for the past ~6800 years, on the higher end of previous estimates (e.g., Khrenov et al. 1991). This rate is close to the estimated Holocene average magma output rate of volcanism in the CKD of 0.042 km^3/year (Melekestsev 1980), and is about one order of magnitude higher than the magma output rate at other arc volcanoes of <0.002 to 0.005 km^3/year (e.g., Hora et al. 2007). Short-term magma output rates in Klyuchevskoy are somewhat smaller but comparable to magma output rates in mantle-plume-related Hawaiian volcanism (0.1–0.18 km^3/year; Cayol et al. 2000).

Such high magma output rates and frequent (once every 2 years, on average) eruptions from Klyuchevskoy indicate a nearly constantly rising magma column, and short-term pre-eruptive magma storage in ephemeral subvolcanic magma reservoirs. This makes Klyuchevskoy comparable to Hawaiian volcanoes such as Kilauea and its magma plumbing system (e.g., Garcia et al. 1998). There, in the complex network of the magma plumbing system, magma mixing and recycling of olivine from cumulates takes place.

Olivine recycling processes under Klyuchevskoy

Oxygen isotope disequilibrium of up to 1‰ from estimated olivine-host glass equilibria and Fe–Mg disequilibria between olivines and their groundmass (Figs. 10, 11) provides the strong evidence for olivine recycling within Klyuchevskoy through mechanisms of magma mixing and/or cumulate entrainment. It is noteworthy that the greatest heterogeneity is observed in samples of intermediate compositions, suggesting that mixing between high-Mg and high-Al magmas commonly generates magmas with diverse olivine populations. We may distinguish magma mixing from olivine cumulate addition by using linear mixing trends on Fig. 9. Magma mixing between high-Al, higher-$\delta^{18}O$ and high-Mg, lower-$\delta^{18}O$ magmas, both with equilibrium olivines, would generate near linear trends and more regular olivine–groundmass $\Delta^{18}O$ relationships that plot closer to equilibrium on Fig. 10. On the other hand, recycling of variable $\delta^{18}O$ olivine cumulates does not have to obey such constraints, and the majority of disequilibrium olivines are better explained by entrapment of high-$\delta^{18}O$ cumulates in lower $\delta^{18}O$ magma and vice versa.

The olivine-melt isotopic and chemical disequilibria in high-$\delta^{18}O$ Klyuchevskoy magmas are similar in magnitude to the low-$\delta^{18}O$ disequilibria discovered in the Laki eruption of Iceland (Bindeman et al. 2006). By comparison with Laki, Fe–Mg and $\delta^{18}O$ re-equilibration of olivine by diffusion after mixing happens on timescales of months to years (e.g., Costa and Dungan 2005) and hundreds of years, respectively. Severe Fe–Mg disequilibria in Klyuchevskoy calls for shorter timescales, consistent with syneruptive (or shortly before eruption) magma mixing processes (consistent with interval between eruptions) during ascent of both magma types from upper crustal reservoirs (≤5 kbar: depths constrained by H_2O–CO_2 contents in melt inclusions) to the surface. Coeval eruption of both high-Al and high-Mg basalt types within some individual eruptions supports this evidence that magma mixing happens syneruptively or shortly before eruption and that the two magma types may share proximal magma plumbing pathways.

Mantle sources and crustal assimilation

Peridotite vs. pyroxenite mantle source

Determination of the source characteristics for Klyuchevskoy magmas is necessary for understanding the exceptionally high $\delta^{18}O$ values. In particular, one possibility that needs to be evaluated is whether the high-Al basaltic magmas are derived from melting of a high-$\delta^{18}O$ pyroxenitic source. The $\delta^{18}O$ values of olivine-free pyroxenites formed by reaction of slab-derived melts with the mantle wedge could be high because the slab-derived melts come from the upper portions of the oceanic crust, which is altered at low temperature by sea water (Muehlenbachs 1986; Staudigel et al. 1995). For example, adakitic melts with moderately high-$\delta^{18}O$ at Shiveluch volcano north of Klyuchevskoy (Bindeman et al. 2005; Portnyagin et al. 2007b) have been inferred to be slab melts (Yogodzinski et al. 2001).

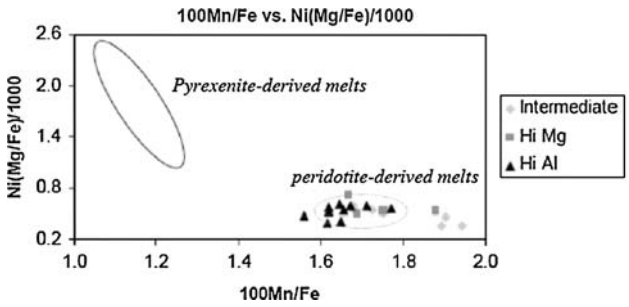

Fig. 16 Trace element concentration ratios in olivines plotted on peridotite–pyroxenite discrimination diagram (Sobolev 2007). Data from this study clearly falls in the peridotite source field

Sobolev (2007) demonstrated that melts derived from pyroxenite, formed by reaction of silicic melts with mantle peridotite, have higher Ni and lower Mn at similar Mg# compared to peridotite-derived melts. Pyroxenite vs. peridotite sources of melts can thus be deciphered by using primitive olivine compositions. We observe that the Klyuchevskoy olivines plot solidly within the peridotite field, which precludes their derivation from an olivine-free pyroxenite mantle (Fig. 16). Furthermore, we notice that Klyuchevskoy basalts are characterized by low Nb concentrations (Fig. 14), which suggests melting of a relatively depleted mantle wedge (Portnyagin et al. 2007a). We conclude that a peridotite-derived melt is a requirement for all Klyuchevskoy magma types.

Assimilation of amphibolite

Next we examine the possibility that assimilation of high-$\delta^{18}O$ lower crustal amphibolite by mantle-derived high-Mg magmas is responsible for the high-$\delta^{18}O$ values (and perhaps water contents) at Klyuchevskoy. Contamination by amphibolite could happen by two different mechanisms: (1) bulk digestion of amphibolite by basaltic magmas or (2) partial melting of the amphibolite and mixing of the melt with basaltic magma. Low degree partial melts of amphibolite at lower crustal pressures tend to be relatively silica-rich, but higher degree melts (>40%) can have high-Al basaltic compositions similar to the high-Al Klyuchevskoy basalts, and with similar H_2O contents (Rapp and Watson 1995).

Despite the reasoning laid out above, there are two main problems with the hypothesis that lower crustal amphibolite assimilation beneath Klyuchevskoy is responsible for the high $\delta^{18}O$ values. First, the amount of assimilation that would be required even to account for the $\delta^{18}O$ values of the primitive, high-Mg basalts is about 20–40% (Bindeman et al. 2004). Such large amounts of assimilation would change the composition of the resulting hybrid basaltic magmas such that they would no longer be primitive, and the compositions of olivine crystals formed by such melts would no longer fall in the peridotite field shown in Fig. 16. Second, the $^{87}Sr/^{86}Sr$ values of analyzed amphibolites from Kamchatka (Bindeman et al. 2004) are relatively high (≥0.7058) compared to the values for high-Mg (0.70355) and high-Al (0.70366) basalts (Kersting and Arculus 1994; Dorendorf et al. 2000). The large amounts of amphibolite assimilation required by the oxygen isotope data would shift the $^{87}Sr/^{86}Sr$ values of Klyuchevskoy basalts to higher values than are observed, unless there are amphibolites in the lower crust beneath this region that have much lower $^{87}Sr/^{86}Sr$ than the analyzed amphibolites from elsewhere in Kamchatka. For these reasons we conclude that the high $\delta^{18}O$ values of Klyuchevskoy basaltic magmas are not caused by lower crustal assimilation but instead must have a subcrustal origin.

Evidence for high primary melt H_2O contents in Klyuchevskoy magmas

We have found evidence for a range of H_2O contents from <1.0–7.1 wt%, with the majority of values between 2 and 5 wt%. Because much of this variation is likely the result of degassing during ascent and crystallization, it is difficult to assess how H_2O contents vary with degree of differentiation. Using our maximum H_2O concentration of 7.1 ± 1.1 wt% in a high-Al melt inclusion in Fo_{80} olivine, we can estimate the maximum H_2O concentration of a primitive melt that would be in equilibrium with a peridotite source. MELTS modeling of fractional crystallization of an olivine-clinopyroxene assemblage requires 25% fractional crystallization from a parental melt in equilibrium with Fo_{90} olivine. Using this value, we estimate a maximum of 5.3 ± 0.8 wt% H_2O in primitive basaltic magma at Klyuchevskoy. This estimate is higher than our highest measured values for high-Mg melt inclusions (maximum 3.9 wt% H_2O in Fo_{88} olivine).

Origin of high-$\delta^{18}O$ in the peridotite source of Klyuchevskoy magmas

One hypothesis for the origin of the high $\delta^{18}O$ values of Klyuchevskoy basaltic magmas involves flux melting of the mantle wedge by addition of high-$\delta^{18}O$ slab-derived fluids or melts. We computed (Fig. 17, see figure caption for computation schemes) a simple mass balance for the required amount of slab-derived H_2O-rich material added to the mantle wedge using various plausible $\delta^{18}O$ values of the slab-derived fluid or hydrous melt. The maximum $\delta^{18}O$ in H_2O-rich fluid or silicate melt that could be inherited from the upper portion of the subducted slab in front of Kamchatka is 8–10‰ for altered basalts (Bailey 1996) and 10–20‰ for sediments (Bindeman et al. 2004). Because water has more oxygen on a molar basis than silicate melt,

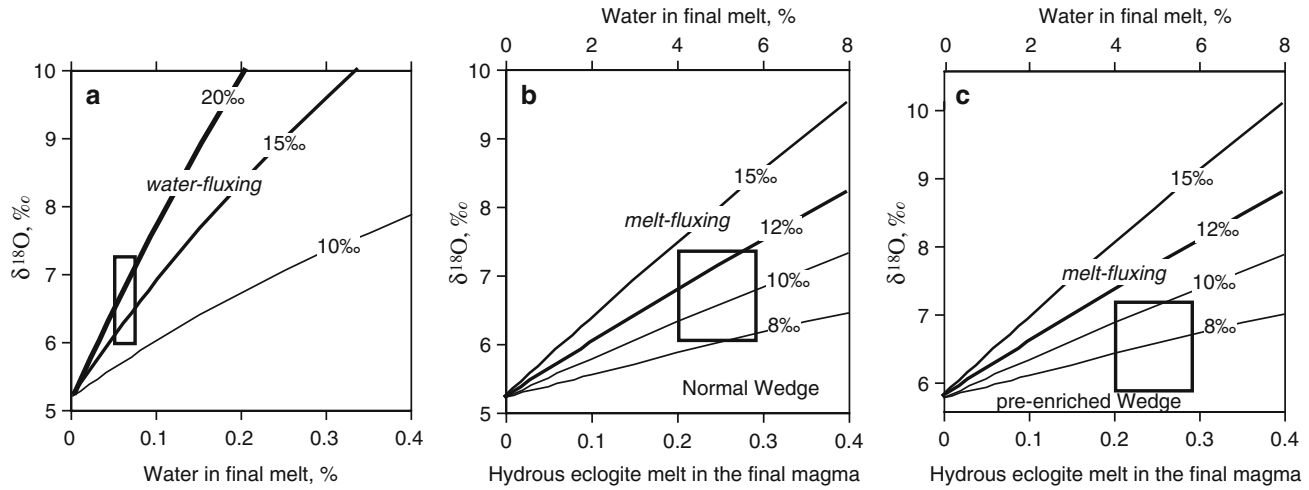

Fig. 17 Mass balance calculations for addition of high-$\delta^{18}O$ fluid or high-$\delta^{18}O$ hydrous melt to either **a, b** normal-$\delta^{18}O$ peridotite or **c** pre-enriched, higher $\delta^{18}O$ peridotite. All calculations are based on a physical model similar to that of Grove et al. (2006) in which fluid or hydrous melt with 20 wt% water rises through the inverted thermal gradient in the mantle wedge, forming small amounts of H_2O-rich melt at the H_2O-saturated solidus. This melt continues to rise into the hotter part of the wedge, dissolving additional anhydrous basaltic components from the peridotite, and lowering the melt H_2O content. In **a** the isotope effects of pure water addition are shown and would require water to be +20‰ or more to match Klyuchevskoy's highest $\delta^{18}O$ compositions (shown by *small rectangle*). In **b**, hydrous dacitic melt is assumed to contain 20 wt% H_2O, which is reduced to the final melt H_2O contents shown along top of figure by dilution with basaltic components derived from peridotite wallrock. The calculation in **c** is similar to **b** except we assume that the starting mantle wedge is enriched by 0.5‰ relative to normal mantle values. Calculations for the isotope effects due to addition of hydrous melt or water used a simple equation: $\delta^{18}O_{\text{final magma}} = [F \times \delta^{18}O_{\text{fluidt}} \times f + (1-f) \times \delta^{18}O_{\text{magma}}]/[F \times f + (1-f) \times M]$, where F and M is the molar proportion of oxygen in hydrous melt (0.57) calculated from the molar proportion of pure water ($F = 0.89$) in anhydrous magma ($M = 0.47$). Note that to make Klyuchevskoy high-$\delta^{18}O$ olivines in melts generated by single stage flux-melting (**a, b**), very high $\delta^{18}O$ values of fluid or melt are required. We favor model (**c**), which involves a pre-enriched mantle wedge composition. See text for discussion

fluxing with solute-free, pure water can generate the high-$\delta^{18}O$ values of olivines of up to 7.2‰, but only if we assume extreme (+20‰ or higher) $\delta^{18}O$ values for the fluid. Addition of 5.5–7.0% of such fluid to normal mantle with $\delta^{18}O_{\text{olivine}} = 5.2$‰ would be required (Fig. 17). While such high $\delta^{18}O$ values for slab-derived fluids were proposed for subduction zones (e.g., Eiler et al. 2000), we consider them extreme and not appropriate for the majority of the subducted sediments beneath Kamchatka. Only marine-precipitated carbonate with $\delta^{18}O$ values as high as +25‰ would be capable of explaining such high $\delta^{18}O$ values at Klyuchevskoy. However, no significant carbonate is found in sediments offshore from Kamchatka (e.g., Bailey 1996) suggesting that a high-$\delta^{18}O$ marine-precipitated component is absent in front of the Kamchatka arc.

Instead of excessively high $\delta^{18}O$ H_2O-rich fluids as required above, Dorendorf et al. (2000) proposed a model of time-integrated fluid addition without melting, in which peridotite is progressively enriched in ^{18}O by multiple episodes of fluid addition. While such a model is theoretically possible, it should yield unusually high fluid-mobile element signatures (e.g., high Ba/La) and should also result in much higher magmatic H_2O than our measured values. Our ion microprobe analyses of the melt inclusions show no evidence for such high fluid-mobile element signatures (Supplementary Table 2). Furthermore, for our measured H_2O contents, the Dorendorf et al. model would require that H_2O was continuously lost from the wedge after each episode of fluid addition, but how this would occur or how so much H_2O is fluxed through the wedge without causing melting was not discussed in their study.

Another possibility is fluxing of the mantle wedge with moderately high-$\delta^{18}O$ hydrous melt derived by slab melting (Fig. 17b). The total amount of hydrous slab melt added to the wedge must be sufficiently small for the final source material for Klyuchevskoy magmas to retain a peridotite signature in terms of bulk mineralogy and Mg/Fe, Ni, and Mn concentrations in olivine (Fig. 16). Based on a simple mass balance of silica and assuming that added melt is dacitic (adakitic) in composition (65% SiO_2), then the maximum amount of such melt added must be less than 33% to retain a peridotitic and not pyroxenitic assemblage. If we assume 20% of such melt added to satisfy HFSE trace element concentrations (e.g., Portnyagin et al. 2007b), then the dacitic melt should contain 20–25% water to match our water concentrations. A slab-melt component, if variably added to the peridotitic mantle wedge, could explain major and trace element differences between volcanoes (Portnyagin et al. 2007a,2007b). Because of the large proportion of previously depleted, olivine-rich peridotite in these mixing models, no clear adakitic signatures would be present except in the northernmost, slab edge volcanoes

such as Shiveluch, Zarechny, and Kharchinsky (Bindeman et al. 2005) whose source would be primarily slab melt. A hydrous melt, rather than hydrous fluid is preferred in our modeling (Fig. 17b), because significant proportion of ^{18}O is carried by the silicate component, without making the final magma unrealistically water-rich.

However, the dacitic melt component would have to be fortuitously high in $\delta^{18}O$ ($\sim$12 to +15‰, Fig. 17b) to match the $\delta^{18}O$ of the final basaltic magma with 7.6‰ olivine that we find at Klyuchevskoy. A global survey of adakitic melts (Bindeman et al. 2005) suggest that only in areas of active sediment melting such as in Setouchi, Japan, could melts be that high in $\delta^{18}O$. We therefore conclude that the highest $\delta^{18}O$ values that we found in primitive magmas at Klyuchevsloy cannot be explained by any one-stage process of fluid or melt addition although the latter fits the mass balance better. A two step process involving prior mantle wedge enrichment of at least 0.5–1‰ (Fig. 17b, c) is required. Then, a slab-derived dacitic melt component of +8 to +10‰ can explain $\delta^{18}O$ values of final basalts and basaltic andesites, and also somewhat elevated silica content for given MgO. These +8 to +9‰ values are common in the upper basaltic portions of the subducted slab (e.g., Muehlenbachs 1986).

Inheritance of high-$\delta^{18}O$ signature from prior mantle enrichment

We suggest that a pre-existing high-$\delta^{18}O$ peridotitic magma source is required to explain Klyuchevskoy magma petrogenesis. The high-$\delta^{18}O$, H_2O-rich subduction-derived component that reaches its extreme beneath Klyuchevskoy is variably present in other volcanoes of the CKD (Portnyagin et al. 2007a), throughout Kamchatka (Bindeman et al. 2004), and in the rear-arc in particular (Duggen et al. 2007). It is particularly characteristic for back-arc volcanoes to the south such as Opala, Koryaksky, and Kizimen, and overall the $\delta^{18}O$ values of mafic volcanic rocks increase across the presently active arc, but then decrease in now extinct Sredinny Range (I.N. Bindeman, unpublished data). To explain this feature, we suggest that magmas in the CKD tap a higher-$\delta^{18}O$ mantle source that was extensively serpentinized over millions of years by high-$\delta^{18}O$ fluids derived from the slab when the mantle now beneath the CKD was part of the Kamchatka forearc, the model favored in the recent review of the CKD volcanism by Portnyagin et al. (2007b) and developed further in this study.

The accretion of eastern cape-peninsulas onto Kamchatka several million years ago (Konstantinovskaia 2001; Lander and Shapiro 2007) stalled subduction, causing the trench to roll back to its present position (Fig. 18). This subduction jump exposed a previously fluxed forearc region in the mantle wedge to rising basaltic magmas in the present subduction configuration. In this subduction jump model, the level of ^{18}O enrichment is expected to be variable along the arc. The previously stronger fluxed and serpentinized areas, additionally affected by large high-$\delta^{18}O$ fluid fluxes from the subducting Hawaii-Emperor chain (Fig. 1; e.g., Kersting and Arculus 1995; Dorendorf et al. 2000; Churikova et al. 2001), led to ^{18}O-rich and hydrous mantle under the present CKD and Klyuchevskoy in particular.

In the proposed model (Fig. 18) a high-$\delta^{18}O$ signature (higher by 0.5–1‰) characterizes the upper mantle, just below the Moho, where rising basaltic liquids generated by flux melting of the mantle wedge may pond during ascent. The ascending hydrous mafic melts under Klyuchevskoy in the present subduction configuration (melts 1–2, Fig. 18c) are capable of digesting significant volumes of high-$\delta^{18}O$, previously hydrated but now deserpentinized, peridotitic mantle (melt 3, Fig. 18c). Their independent eruption and intermixing (melt 4, Fig. 18c) creates chemical and isotopic diversity seen in Klyuchevskoy volcano. Unlike the classic MASH process under island arcs, in which basaltic magmas assimilate lower crustal arc roots (e.g., Hildreth and Moorbath 1988; Ducea and Barton 2007) to create high-$\delta^{18}O$ values in silicic volcanic rocks, we propose an analogous process that occurs with high-$\delta^{18}O$ lithospheric mantle peridotite. A complication to our hypothesis is that thermal models for the mantle wedge (Manea et al. 2007) suggest temperatures in the uppermost mantle that are too high for serpentine and probably chlorite to be stable (Grove et al. 2006). Therefore, previously hydrated forearc mantle would have been heated after the slab jump, driving off H_2O and some fluid mobile elements during deserpentinization but retaining high $\delta^{18}O$. Lack of correlation between water in melt inclusions and $\delta^{18}O_{olivine}$ values in our dataset suggests decoupling, and thus are unlikely part of the single stage, flux melting process. We suggest that the highest-$\delta^{18}O$ signature of Klyuchevskoy's high-Al basalt and its high-Mg parent, was inherited from deserpentinized old ($\geq$5 Ma) lithospheric mantle with subtly higher $^{87}Sr/^{86}Sr$ isotopes. High concentrations of water in a variety of primitive Klyuchevskoy melts originate from melting of mantle wedge fluxed by fluids liberated from the presently subducting Emperor Seamounts (Fig. 18).

Mantle xenolth studies of Kamchatkan subarc mantle (e.g., Kepezhinskas et al. 2002; Ishimaru et al. 2004; Ionov and Seitz 2008 and references therein) provide evidence for hydrous to adakitic, melt like fluids that caused transformation of olivine to pyroxene that is rich in fluid inclusions. However no oxygen isotopic studies have been yet performed on the Kamchatkan xenoliths to whether they have high-$\delta^{18}O$ values, and this should be the objective of the next study.

The isotopic and chemical differences that we observe between high-Al and high-Mg basalts can be explained by

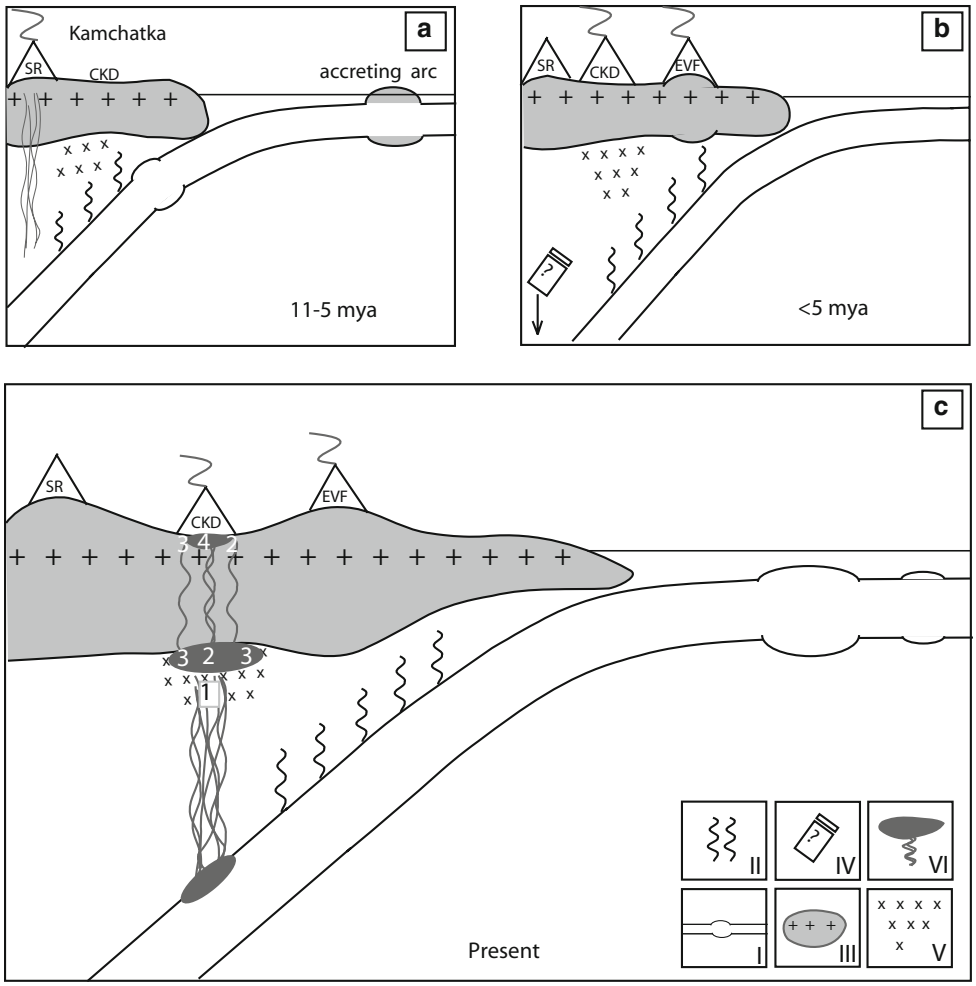

Fig. 18 Schematic diagram of the evolution of Kamchatka and the corresponding processes involved from active volcanism at the Sredinny Ridge (SR) to the formation of Central Kamchatka Depression (CKD) volcanoes and the Eastern Volcanic Front (EVF) from **a** 11–5 ma, **b**<5 ma, **c** present. In these diagrams: *I* Hawaii-Emperor Seamounts, *II* fluid, *III* continental or arc crust, *IV* separated piece of subducted slab, *V* serpentinized peridotite, *VI* melt. In figure **c** four types of melt are present: *1* primary melt with slab and peridotite components, not seen on the surface; *2* moderately high-$\delta^{18}O$, high-Mg basaltic andesite evolved primarily from 1; *3* upper mantle high-Al, very high-$\delta^{18}O$, high-$^{87}Sr/^{86}Sr$ basalt evolved primarily from previously enriched, highest-$\delta^{18}O$ deserpentinized mantle wedge; and *4* mixing of high-Mg and high-Al cumulates with basalt and basaltic andesite 2 and 3 upon rise

this proposed model. High-Al, higher-$\delta^{18}O$, higher $^{87}Sr/^{86}Sr$ basalts involve a larger component from the older, previously hydrated peridotitic component, whereas the high-Mg basalts at Klyuchevskoy contain less of this component. Both melts erupt coevally and mix to variable degrees upon ascent. This model provides a mechanistic interpretation for the complex olivine recycling processes that we have documented. Olivine recycling happens in upper crustal magma chambers and also during ascent and mixing of the different magma types.

Comparison with previous models

The present study presents a tectonic and geochemical model that is different from those published earlier (Dorendorf et al. 2000; Churikova et al. 2001) because it requires a subduction jump to explain the extremely high-$\delta^{18}O$ magma signature (Fig. 18) and its inheritance from previously hydrated forearc mantle. In our earlier treatment of high-$\delta^{18}O$ basic rocks of Kamchatka we ascribed the high-$\delta^{18}O$ signature of more evolved magmas Kamchatka-wide to assimilation and melting of high $\delta^{18}O$ basic arc roots (Bindeman et al. 2004). Without denying this possibility for more evolved rocks outside of the CKD, we suggest that for rather primitive basalts and basaltic andesites with forsteritic olivines, an ultramafic high-$\delta^{18}O$ assimilant is required. A deserpentinized peridotite, fluxed previously by high-$\delta^{18}O$ fluids as a part of the former forearc region before the subduction jump, fits the profile well.

Therefore, the main conclusion of this paper is that the volcanism is put into the tectonic context of a subduction jump, and is not due to the excessive or time-integrated fluid flux. The rarity of high-$\delta^{18}O$ magmas worldwide suggest that "special" tectonic regimes are required to explain the origin of these magmas. As other volcanoes in the CKD are high-$\delta^{18}O$, this model finds regional support.

Comparison with Mt Shasta: a high-$\delta^{18}O$, H_2O-rich cascade volcano

Comparison with Mt Shasta is warranted because in both places high magma production rates are coupled with high-$\delta^{18}O$ signatures and high H_2O contents (Grove et al. 2002,

2006; Bindeman et al. 2005; Martin et al. 2008). A key to understanding the cause of high-$\delta^{18}O$ magmas at Klyuchevskoy can be found by examining anomalies present at both subduction zones. For Klyuchevskoy, subduction of the Hawaii-Emperor chain caused earlier strong serpentinization of the forearc mantle wedge (prior to subduction jump) and continues to supply fluid from the slab into the wedge to cause flux melting. Through these processes, the overthickened oceanic crust of the Hawaii-Emperor chain is responsible for the particularly high-$\delta^{18}O$ values and high H_2O contents, higher than in the rest of Kamchatka (e.g., Bindeman et al. 2004; Duggen et al. 2007). For Mt Shasta, however, it is the presence of the subducting Blanco fracture zone, which likely creates enhanced permeability of sea water within the oceanic lithosphere before subduction, resulting in low temperature hydrothermal alteration of a larger than normal fraction of the crust. This crust, on subduction, would therefore release a larger amount of high-$\delta^{18}O$ fluids, and thus possibly account for the high-$\delta^{18}O$ signature documented at Mt Shasta (Martin et al. 2008). It is also possible that upper lithospheric contamination by the high-$\delta^{18}O$ deserpentinized ultramafic rocks contributed high-$\delta^{18}O$ signature to the Mt Shasta rocks, although $\delta^{18}O$ values and mass balance are less extreme for Mt Shasta to require that. It should also be noted that subvolcanic interaction with regionally abundant Trinity ultramafic complex will not produce the required torque on Mt Shasta oxygen isotopes as the Trinity rocks are low-$\delta^{18}O$ (Martin et al. 2008). Therefore, for Klyuchevskoy and Mt Shasta cases, we suggest that petrogenetic processes involve hydrous flux melting and larger than normal amounts of H_2O derived from subducted oceanic crust and sublithospheric interaction with the pre-existing high-$\delta^{18}O$ ultramafic rocks.

Conclusions

The results of this study have served to explain Klyuchevskoy's (1) voluminous, high-rate volcanism, (2) the unusual high-$\delta^{18}O$ signature of Klyuchevskoy and other CKD rocks and (3) the H_2O-rich nature of both the high-Mg and the high-Al high-$\delta^{18}O$ basaltic components. The processes involved in magma generation below Klyuchevskoy volcano are more complicated then previously interpreted. Major element data show the presence of both high-Al and high-Mg basaltic magma types as well as intermediate products. These products are strongly enriched in ^{18}O ($\delta^{18}O_{olivine}$ of up to 7.6‰), particularly the high-Al basalt. Olivine-hosted melt inclusions in high-Al samples are H_2O-rich, and contain up to 7.1 wt% water, but melt inclusions in high-Mg samples are also relatively H_2O-rich, with up to 3.9 wt% H_2O. Many samples have groundmass glass that is isotopically and chemically out of equilibrium with their olivines, indicating that olivine recycling between variable $\delta^{18}O$ cumulate and magma (see above) is a likely process at Klyuchevskoy.

We have shown that fluids or slab melts derived from the subducted Hawaii-Emperor Seamount chain crust within the present day subduction configuration cannot explain the required $\delta^{18}O$ enrichment of volcanic rocks at Klyuchevskoy. Fluid fluxing of peridotite requires extremely high-$\delta^{18}O$ values for single-stage flux-melting, and multi-stage flux melting models would result in extremely high fluid mobile/immobile element signatures, which are not seen at Klyuchevskoy. Melt fluxing is a better explanation but the $\delta^{18}O$ values of such melt strain the mass balance. Simple fractionation of a primitive, high-Mg, normal-$\delta^{18}O$ basalt will only increase the $\delta^{18}O$ of derivative high-Al basaltic magmas on the order of 0.1–0.3‰, and cannot account for the several permil enrichment above mantle values evident at Klyuchevskoy. Involvement of a high-$\delta^{18}O$ pyroxenite mantle source was ruled out because Mg/Fe, Ni, and Mn values indicate a peridotite source. Amphibolite assimilation models likewise could not provide a consistent model to account for observed $\delta^{18}O$ and $^{87}Sr/^{86}Sr$ values. Examination of published values for ^{10}Be and $^{207}Pb/^{204}Pb$ and $^{208}Pb/^{204}Pb$ ratios pertaining to sediment subduction shows no evidence of a significant contribution. Therefore, we present a hypothesis in which hydrous melt flux melting of the peridotitic mantle wedge creates primitive basaltic melts that rise and interact with higher-$\delta^{18}O$ peridotite in the uppermost mantle that was once hydrated and enriched as part of the forearc mantle prior to trench migration at ~5–2 m.y.a (Lander and Shapiro 2007).

The formation of the high $\delta^{18}O$, high-Al and moderately high $\delta^{18}O$ high-Mg parental melts of Klyuchevskoy volcano likely occurs from the combination of two processes: (1) the release of fluid/melt (probably with moderately high $\delta^{18}O$) from the subducting slab resulting in flux melting of the mantle wedge and generation of primary high-Mg, normal to moderately high-$\delta^{18}O$ basalts enriched in the most fluid-mobile elements and (2) interaction of the ascending primary melts with lithospheric mantle with high $\delta^{18}O$ formed by de-serpentinization of old forearc mantle, resulting in a range of $\delta^{18}O$ in high Mg# melts. The key here is that interaction of ascending magma with high-$\delta^{18}O$ ultramafic rock will not change its Mg# but will lead to variable $\delta^{18}O$ in the melt. The high-Al magma type is derived from a parental melt that incorporated a substantial proportion of high-$\delta^{18}O$ shallow mantle, whereas the high-Mg assimilates less of this component. Polybaric fractionation of variably high $\delta^{18}O$ parental melts, their mixing, and cumulate-magma mixing gives the origin for the entire spectrum of Klyuchevskoy rocks ranging from

high-Mg basalts to low-Mg, high-Al basalts with disequilibrium olivines. In our proposed magma generation hypothesis for Klyuchevskoy, trench migration caused by tectonic processes plays a central role in explaining the high-δ^{18}O hydrous basaltic magmatism. Assimilation of shallow hydrothermally altered lithospheric mantle might be a common process to explain the origin of high-δ^{18}O primitive arc rocks, particularly, in the volcanic arcs built on accreted ophiolitic terrains such as for example the Cascadia Arc or Mexican Volcanic Belt.

Acknowledgments This research represents the M.S. thesis by the lead author. It was supported by NSF grants EAR0537872 (Bindeman) and EAR0309559 (Wallace). We thank Jim Palandri for help with stable isotope analyses, John Donovan for help with the electron microprobe, Sergei Simakin and Nikita Mironov for their help with the ion microprobe and sample preparation. We also thank Gerhard Wörner and an anonymous reviewer for their helpful reviews. The KALMAR project from the Ministry of Science and Education of Germany supported M. Portnyagin. Fieldwork was supported by NSF grant EAR 0537872 and in part by grants 06-05-64960 and 06-05-65037 from the Russian Foundation for Basic Research.

References

Almeev RR, Kimura JI, Ozerov AY, Ariskin AA, Barmina GS (2003) From high-Mg basalts to dacites: continued crystal fractionation in the Klyuchevskoy-Bezymianny magma plumbing system, Kamchatka. Geochim Cosmochim Acta 67:A13

Anderson AT (1973) The before-eruption water content of some high-alumina magmas. Bull Volcanol 37:530–552. doi:10.1007/BF02596890

Ariskin AA, Barmina GS, Ozerov AY, Nielsen RL (1995) Genesis of High-Alumina Basalts of Klyuchevskoy Volcano. Petrology 5:496–521

Avdeiko GP, Savelyev DP, Palueva AA, Popruzhenko SV (2007) Evolution of the Kurile–Kamchatka volcanic arcs and dynamics of the Kamchatka–Aleutian junction. In: Eichelberger J, Izbekov P, Kasahara M, Lees J, Gordeev E (eds) Volcanism and tectonics of the Kamchatka Peninsula and adjacent arcs, American Geophysical Union Monograph Series, vol 172, AGU, Washington, pp 37–55

Bailey JC (1996) Role of subducted sediments in the genesis of Kurile–Kamchatka island arc basalts: Sr isotopic and elemental evidence. Geochem J 30:289–321

Bindeman IN, Vinogradov VI, Valley JW, Wooden JL, Natal'in BA (2002) Archean protolith and accretion of crust in Kamchatka: SHRIMP dating of Zircons from Sredinny and Ganal Massifs. J Geol 110:271–289. doi:10.1086/339532

Bindeman IN, Ponomareva VV, Bailey JC, Valley JW (2004) Volcanic arc of Kamchatka: a province with high-delta O-18 magma sources and large-scale O-18/O-16 depletion of the upper crust. Geochim Cosmochim Acta 68(4):841–865. doi:10.1016/j.gca.2003.07.009

Bindeman IN, Eiler JM, Yogodzinski G, Tatsumi Y, Stern C, Grove T et al (2005) Oxygen isotope evidence for slab melting in modern and ancient subduction zones. Earth Planet Sci Lett 235:480–496. doi:10.1016/j.epsl.2005.04.014

Bindeman IN, Sigmarsson O, Eiler JM (2006) Time constraints on the origin of large volume basalts derived from O-isotope and trace element mineral zoning and U-series disequilibria in the Laki and Grímsvötn volcanic system. Earth Planet Sci Lett 245:245–259. doi:10.1016/j.epsl.2006.02.029

Braitseva OA, Melekestsev IV, Ponomareva VV, Sulerzhitsky LD (1995) The ages of calderas, large explosive craters and active volcanoes in the Kurile–Kamchatka region, Russia. Bull Volcanol 57(6):383–402

Braitseva OA, Ponomareva VV, Sulerzhitsky LD, Melekestsev IV, Bailey JC (1997) Holocene key-marker tephra layers in Kamchatka, Russia. Quatern Res 47:125–139. doi:10.1006/qres.1996.1876

Cayol V, Dieterich JH, Okamura AT, Miklius A (2000) High magma storage rates before the 1983 eruption of Kilauea, Hawaii. Science 288:2343–2346. doi:10.1126/science.288.5475.2343

Chiba H, Chacko T, Clayton RN, Goldsmith JR (1989) Oxygen isotope fractionations involving diopside, forsterite, magnetite, and calcite: Application to geothermometry. Geochim Cosmochim Acta 53:2985–2995. doi:10.1016/0016-7037(89)90174-9

Churikova T, Dorendorf F, Worner G (2001) Sources and fluids in the mantle wedge below Kamchatka, evidence for across-arc geochemical variation. J Petrol 42:1567–1593. doi:10.1093/petrology/42.8.1567

Churikova T, Worner G, Mironov N, Kronz A (2007) Volatile (S, Cl and F) and fluid mobile trace element compositions in melt inclusions: implications for variable fluid sources across the Kamchatka arc. Contrib Mineral Petrol 154(2):217–239. doi:10.1007/s00410-007-0190-z

Costa F, Dungan M (2005) Short time scales of magmatic assimilation from diffusion modeling of multiple elements in olivine. Geology 33:837–840. doi:10.1130/G21675.1

Dorendorf F, Wiechert U, Worner G (2000) Hydrated sub-arc mantle: a source for the Klyuchevskoy volcano, Kamchatka/Russia. Earth Planet Sci Lett 175:69–86. doi:10.1016/S0012-821X(99)00288-5

Ducea MN, Barton MD (2007) Igniting flare-up events in Cordillieran arcs. Geology 35:1047–1050. doi:10.1130/G23898A.1

Duggen S, Portnyagin M, Baker J, Ulfbeck D, Hoernle K, Garbe-Schonberg D et al (2007) Drastic shift in lava geochemistry in the volcanic-front to rear-arc region of the Southern Kamchatkan subduction zone: evidence for the transition from slab surface dehydration to sediment melting. Geochim Cosmochim Acta 71:452–480. doi:10.1016/j.gca.2006.09.018

Eiler JM (2001) Oxygen isotope variations in basaltic lavas and upper mantle rocks. Rev Mineral Geochem 43:319–364

Eiler JM, Crawford A, Elliott T, Farley KA, Valley JW, Stolper EM (2000) Oxygen isotope geochemistry of oceanic-arc lavas. J Petrol 41:229–256

Garcia MO, Ito E, Eiler JM, Pietruszka AJ (1998) Crustal contamination of Kilauea volcano magmas revealed by oxygen isotope analyses of glass and olivine from Puu Oo eruption lavas. J Petrol 39:803–817. doi:10.1093/petrology/39.5.803

Ghiorso MS, Sack RO (1995) Chemical mass transfer in magmatic processes. 4. A revised and internally consistent thermodynamic model for the interpolation and extrapolation of liquid-solid equilibria in magmatic systems at elevated temperatures and pressures. Contrib Mineral Petrol 119(2–3):197–212. doi:10.1007/BF00307281

Gorbatov A, Kostoglodov V, Suarez G, Gordeev E (1997) Seismicity and structure of the Kamchatka subduction zone. J Geophys Res 102:17833–17898. doi:10.1029/96JB03491

Gorbatov A, Domínguez J, Suárez G, Kostoglodov V, Zhao D, Gordeev E (1999) Tomographic imaging of the *P*-wave velocity structure beneath the Kamchatka peninsula. Geophys J Int 137(2):269–279. doi:10.1046/j.1365-246X.1999.00801.x

Grove TL, Parman SW, Bowring SA, Price RC, Baker MB (2002) The role of an H2O-rich fluid component in the generation of

primitive basaltic andesites and andesites from the Mt. Shasta region, N. California. Contrib Mineral Petrol 142:375–396

Grove TL, Chatterjee N, Parman SW, Medard E (2006) The influence of H_2O on mantle wedge melting. Earth Planet Sci Lett 249(1–2):74–89. doi:10.1016/j.epsl.2006.06.043

Gurenko AA, Belousov AB, Trumbull RB, Sobolev AV (2005) Explosive basaltic volcanism of the Chikurachki volcano (Kurile arc, Russia): insights on pre-eruptive magmatic conditions and volatile budget revealed from phenocryst-hosted melt inclusions and groundmass glasses. J Volcanol Geotherm Res 147:203–232. doi:10.1016/j.jvolgeores.2005.04.002

Hildreth W, Moorbath S (1988) Crustal contributions to arc magmatism in the Andes of Central Chile. Contrib Mineral Petrol 98:455–489. doi:10.1007/BF00372365

Hora JM, Singer BS, Worner G (2007) Volcano evolution and eruptive flux on the thick crust of the Andean Central Volcanic Zone: Ar-40/Ar-39 constraints from Volcan Parinacota, Chile. Geol Soc Am Bull 119:343–362. doi:10.1130/B25954.1

Ionov DA, Seitz HM (2008) Lithium abundances and isotopic compositions in mantle xenoliths from subduction and intra-plate settings: mantle sources vs. eruption histories. Earth Planet Sci Lett 3–4:316–331. doi:10.1016/j.epsl.2007.11.020

Ishimaru S, Arai S, Ishida T, Shirasaka M, Okrugin VM (2004) Melting and multi-stage metasomatism in the mantle wedge beneath a frontal arc inferred from highly depleted peridotitic xenoliths from Avacha volcano, S Kamchatka. J Petrol 48:395–433. doi:10.1093/petrology/egl065

Johnson E, Wallace PW, Delgado GH, Manea V, Kent A, Bindeman IN, Donegan C (2008) The origin of H^2O-rich subduction components beneath the Michoacán-Guanajuato Volcanic Field, Mexico: insights from magmatic volatile contents, oxygen isotopes, and 2-D thermal models for the subducted slab and mantle wedge. J Petrol (in press)

Kepezhinskas P, Defant MJ, Widom E (2002) Abundance and distribution of PGE and Au in the island-arc mantle: implications for subarc metasomatism. Lithos 60:113–128. doi:10.1016/S0024-4937(01)00073-1

Kersting AB (1991) Petrology and geochemistry of Klyuchevskoy Volcano, Kamchatka, U.S.S.R.; implications for the chemical and physical evolution of island arcs, PhD Dissertation, University of Michigan, Ann Arbor, p 245

Kersting AB, Arculus RJ (1994) Klyuchevskoy volcano, Kamchatka Russia—the role of high-flux recharged, tapped, and fractionated magma chamber(s) in the genesis of high-Al2O3 from high MgO basalt. J Petrol 35(1):1–41

Kersting AB, Arculus RJ (1995) Pb isotope composition of Klyuchevskoy volcano, Kamchatka and North Pacific sediments: implications for magma genesis and crustal recycling in the Kamchatkan arc. Earth Planet Sci Lett 136(3–4):133–148. doi:10.1016/0012-821X(95)00196-J

Khrenov AP, Dvigalo VN, Kirsanov IT, Fedotov SA, Gorel'chik VI, Zharinov NA (1991) Klyuchevskoy volcano. In: Fedotov SA, Masurenkov YP (eds) Active volcanoes of Kamchatka, vol 1. Nauka Publishers, Moscow, pp 104–153

Khubunaya SA, Gontovaya LI, Sobolev AV, Niskous I (2007) Magma chambers beneath Klyuchevskoy group volcanoes. Volcanol Seismol 2:32–54

Konstantinovskaia EA (2001) Geodynamics of an early eocene arc-continent collision reconstructed from the Kamchatka Orogenic Belt, NE Russia. Tectonophysics 325:87–105. doi:10.1016/S0040-1951(00)00132-3

Lander AV, Shapiro MN (2007) The origin of the modern Kamchatka zone. In: Volcanism and subduction: the Kamchatka Region. Geophys Monograph Series, vol 172. AGU, Washington, pp 57–64

Lees JM, Symons N, Chubarova O, Gorelchik V, Ozerov A (2007) Tomographic images of Klyuchevskoy volcano P-wave velocity. In: Eichelberger J, Izbekov P, Kasahara M, Lees J, Gordeev E (eds) Volcanism and tectonics of the Kamchatka Peninsula and adjacent arcs, American Geophysical Union Monograph Series. AGU, Washington, pp 293–302

Levin V, Shapiro N, Park J, Ritzwoller M (2002) Seismic evidence for catastrophic slab loss beneath Kamchatka. Nature 418:763–767. doi:10.1038/nature00973

Manea VC, Manea M, Clark S (2007) Thermal models beneath Kamchaka and the Pacific plate rejuvenation from a mantle plume impact. In: Eichelberger J, Izbekov P, Kasahara M, Lees J, Gordeev E (eds) Volcanism and tectonics of the Kamchatka Peninsula and adjacent arcs, American Geophysical Union Monograph Series. AGU, Washington, pp 77–90

Martin E, Bindeman IN, Grove TL (2008) Subduction in high fluid fluxing environment and the origin of high-d18O lavas in Mt. Shasta, Cascade arc, California (in preparation)

Melekestsev IV (1980) Volcanism and relief formation. Nauka Publishers, Moscow (in Russian)

Mironov NL, Portnyagin MV, Pletchov PY, Khubunaya SA (2001) Final stages of mama evolution in Klyuchevskoy volcano, Kamchatka: evidence form melt inclusions in minerals of high-alumina basalts. Petrology 9(1):51–69

Muehlenbachs K (1986) Alteration of the oceanic crust and the ^{18}O history of seawater. In: JW Valley, HP Taylor, JR O'Neil Jr (eds) Stable isotopes in high temperature geological processes. Rev Mineral 16:425–444

Newman S, Lowenstern JB (2002) VolatileCalc: a silicate melt-H_2O-CO_2 solution model written in Visual Basic for excel. Comput Geosci 28:597–604. doi:10.1016/S0098-3004(01)00081-4

Ozerov AY (2000) The evolution of high-alumina basalts of the Klyuchevskoy volcano, Kamchatka, Russia, based on microprobe analyses of mineral inclusions. J Volcanol Geotherm Res 95:65–79. doi:10.1016/S0377-0273(99)00118-3

Ozerov AY, Ariskin AA, Kyle P, Bogoyavlenskaya GE, Karpenko SF (1997) Petrological–geochemical model for genetic relationships between basaltic and andesitic magmatism of Klyuchevskoi and Bezymyannyi volcanoes, Kamchatka. Petrology 5/6:614–635

Pineau F, Semet MP, Grassineau N, Okrugin VM, Javoy M (1999) The genesis of the stable isotope (O, H) record in arc magmas: the Kamchatka's case. Chem Geol 62:157–176

Piyp VB, Yefimova YA (1993) Seismic sections of the earth's crust under volcanoes of Kamchatka. Int Geol Rev 35:170–177

Pokrovsky BG, Volynets ON (1999) Oxygen-isotope geochemistry in volcanic rocks of the Kurile–Kamchatka arc. Petrology 7:227–251

Ponomareva VV, Melekestsev IV, Dirksen OV (2006) Sector collapses and large landslides on late Pleistocene–Holocene volcanoes in Kamchatka, Russia. J Volcanol Geotherm Res 158:117–138. doi:10.1016/j.jvolgeores.2006.04.016

Ponomareva VV, Kyle PR, Pevzner MM, Sulerzhitsky LD, Hartman M (2007) Holocene eruptive history of Shiveluch volcano. Kamchatka Peninsula. In: Eichelberger J, Gordeev E, Kasahara M, Izbekov P, Lees J (eds) Volcanism and tectonics of the Kamchatka Peninsula and adjacent arcs, American Geophysical Union Geophysical Monograph Series, vol 172. AGU, Washington, pp 263–282

Portnyagin M, Manea VC (2008) Mantle temperature control on composition of arc magmas along the Central Kamchatka Depression. Geology 36(7):519–522. doi:10.1130/G24636A

Portnyagin M, Hoernle K, Avdeiko GP, Hauff F, Werner R, Bindeman IN et al (2005) Transition from arc to oceanic magmatism at the Kamchatka–Aleutian junction. Geology 33(1):25–28. doi:10.1130/G20853.1

Portnyagin M, Hoernle K, Plechov P, Mironov N, Khubunaya S (2007a) Constraints on mantle melting and composition and nature of slab components in volcanic arcs from volatiles (H_2O, S, Cl, F) and trace elements in melt inclusions form the Kamchatka Arc. Earth Planet Sci Lett 255:53–69. doi:10.1016/j.epsl.2006.12.005

Portnyagin M, Bindeman IN, Hoernle K, Hauff F (2007b) Geochemistry of primitive lavas of the Central Kamchatka depression: magma generation at the edge of the Pacific Plate. In: Eichelberger J, Izbekov P, Kasahara M, Lees J, Gordeev E (eds) Volcanism and tectonics of the Kamchatka Peninsula and adjacent arcs, American Geophysical Union Monograph Series, vol 172. AGU, Washington, pp 199–239

Rapp RP, Watson EB (1995) Dehydration melting of metabasalts at 8–32 kbars: implications for continental growth and crust-mantle recycling. J Petrol 36:891–931

Sobolev AV, Chaussidon M (1996) H_2O concentrations in primary melts from suprasubduction zones and mid-ocean ridges: implications for H_2O storage and recycling in the mantle. Earth Planet Sci Lett 137:45–55

Sobolev AV, Hofmann, AW, Kuzmin DV et al (2007) The amount of recycled crust in sources of mantle-derived melts. Science 316:412–417. doi:10.1126/science.1138113

Spilliaert N, Allard P, Metrich N, Sobolev V (2006) Melt inclusion record of the conditions of ascent, degassing, and extrusion of volatile-rich alkali basalt during the powerful 2002 flank eruption of Mount Etna (Italy). J Geophys Res. Series/Report no.:/111. doi:10.1029/2005JB003934

Staudigel H, Davies GR, Hart SR, Marchant KM, Smith BM (1995) Large-scale isotopic Sr, Nd and O isotopic anatomy of altered oceanic crust-DSP/ODP sites 417/418. Earth Planet Sci Lett 130:169–185. doi:10.1016/0012-821X(94)00263-X

Sun SS, McDonough WF (1989) Chemical and isotopic systematics of oceanic basalts: implications for the mantle composition and processes. In: Magmatism in the Ocean Basin, vol 42. Geol Soc Sp Publ. Geological Society, London, pp 313–345

Volynets ON (1994) Geochemical types, petrology and genesis of late Cenozoic volcanic rocks from the Kurile–Kamchatka island-arc system. Int Geol Rev 36(4):373–405

Wallace PJ (2005) Volatiles in subduction zone magmas: concentrations and fluxes based on melt inclusion and volcanic gas data. J Volcanol Geotherm Res 140:217–240. doi:10.1016/j.jvolgeores.2004.07.023

Yogodzinski GM, Lees JM, Churikova TG, Dorendorf F, Woerner G, Volynets ON (2001) Geochemical evidence for the melting of subducting oceanic lithosphere at plate edges. Nature 404:500–504. doi:10.1038/35054039

APPENDIX A

SAMPLING AND ANALYTICAL METHODS

Sampling of Klyuchevskoy Tephra and Lava

Lavas available for sampling at lower altitudes on Klyuchevskoy's slopes erupted primarily from flank vents and thus cover only the most recent ~3500 years of activity. Lavas erupted from the summit crater are covered with thick pyroclastic, landslide and lahar deposits and are exposed only in the chutes high on the edifice (Ponomareva et al. 2006). Locations of lava flows and cinder cones sampled for this study are shown in **Fig. 3** in the min paper**.** In contrast to previous petrologic and geochemical studies, we focused primarily on Klyuchevskoy tephra. Advantages of tephra studies include complete coverage of the eruptive history, age control of the samples using dated marker ash layers (**Fig. 4**, Braitseva et al. 1997), and good preservation of melt inclusions due to rapid quenching of tephra.

Proximal Klyuchevskoy tephra consist of dark gray cinders ranging from sand-sized ash to lapilli and bombs. Rapidly accumulated cinder horizons are interbedded with thin paleosols to form a dark gray sequence, which contains, in addition, well-defined light colored silicic maker tephra layers from different Kamchatka volcanoes (**Fig. 4**). Most of the lapilli-sized cinders erupted from flank vents rather than the summit crater. Cinder layers range from a few mm to 1 m in thickness, depending on the strength of the eruption, proximity of the vent, and the wind direction at the time of the eruption. A single outcrop may contain thousands of years of volcanic deposits that are not represented or available for sampling in the lava record. ^{14}C-dated marker tephra layers (Braitseva et al. 1997, Ponomareva et al. 2007) provide age estimates for intercalated tephra or lava deposits in the sections that we sampled.

A few cinder layers at the bottom of the Holocene tephra sequences dramatically differ in composition from Klyuchevskoy rocks and represent early Holocene Plosky volcano activity. These layers are probably related to formation of Plosky's most recent summit caldera at ~8600 BP (Braitseva et al. 1995). The deposits of these compositionally distict and more alkalic eruptions are represented by a widespread package of cinder layers, a number of large cinder cones, and the extensive Lavovy Shish lava field (**Fig. 2-3**). The oldest sampled Holocene products overlie glacial till and the late Pleistocene lava pedestal.

Fig. 5 shows the stratigraphy of the sections we sampled and the marker beds that were used for tephrochronology. Tephra samples for this study come from several riverbank outcrops around the NE quadrangle of Klyuchevskoy volcano (**Fig. 2 and 3**) and include the nearly entire Holocene record of mafic explosive volcanism in the area. In this work we sampled only tephra layers thicker than 5 cm, with lapilli ≥1 mm, and which exhibited no sorting by water. Sand sized and smaller particles were not analyzed due to the possibility of aeolian segregation and mixing of multiple deposits.

Analytical Methods

Oxygen isotope analyses were performed at the University of Oregon stable isotope lab using CO_2-laser fluorination. Individual and bulk mineral grains ranging in weight between 0.6 and 2 mg were reacted in the presence of purified BrF_5 reagent to liberate oxygen. The gas generated in the laser chamber was purified through a series of cryogenic traps held at liquid nitrogen temperature, and a mercury diffusion pump was used to remove traces of fluorine gas. Oxygen was converted to CO_2 gas in a small platinum-graphite converter, the yield was measured, and then CO_2 gas was analyzed on a MAT 253 mass spectrometer. Four to seven standards were analyzed together with the unknowns during each analytical session. San Carlos olivine ($\delta^{18}O$ = 5.35‰) and Gore Mt. Garnet ($\delta^{18}O$

= 5.75‰) were used. Day-to-day $\delta^{18}O$ variability of standards ranged from 0.1 to 0.25‰ lighter than their reference values. Measurements of unknowns were appropriately adjusted to correct for this variability. The average precision on standards and duplicates of individual olivine analyses is better than 0.1‰.

Melt inclusions (MI) in olivine were analyzed for H_2O and CO_2 using Fourier Transform Infrared Spectroscopy (FTIR) at the University of Oregon. Over 40 melt inclusions in 7 tephra samples were identified, doubly intersected, and polished down to wafers 12-80 microns thick, depending on the size of the inclusion and olivine host. The thickness of each MI was determined by visual measurement under a petrographic microscope and in some cases by measurement of interference fringe spacing in reflectance spectra (Nichols and Wysoczanski 2007). Total dissolved H_2O was measured from the intensity of the asymmetric band at 3550 cm^{-1}, and dissolved CO_3^{2-} was measured using peaks at 1515 and 1430 cm^{-1}. The concentration (*c*) of a species was then calculated using Beer's Law: $c = MA / \rho l \varepsilon$, where *M* is the molecular weight of the species, *A* is the IR absorbance of the species, ρ is the density of the glass inclusion, *l* is the thickness of the inclusion, and ε is the molar absorption coefficient. The density was estimated initially by assuming an anhydrous composition, and then iteratively revised through calculation of the H_2O content of the glass and hydrous glass density (Luhr, 2001). The molar absorption coefficient for H_2O was 63 ± 3 L/mol cm (Dixon et al. 1995). Since the absorption coefficient for the carbonate doublet at 1515 and 1430 cm^{-1} is compositionally dependent, it was calculated for each sample using the major element compositions of the melt inclusions and the linear equation in Dixon and Pan (1995). Duplicate IR spectra were acquired for each melt inclusion. Corrections were made for post-entrapment crystallization of the melt inclusions (e.g. Sobolev and Shimizu 1993), with most inclusions requiring less than 4% olivine addition and a maximum of 15%. Melt inclusions were also examined for diffusive loss of iron by comparing MgO vs. FeO^T of whole rock, bulk tephra, and matrix glass data with the corrected melt inclusion values (e.g. Danyushevsky et al. 2002). We concluded that diffusive loss of iron from the melt inclusions was negligible, except for inclusion KLV5/18a (Table 2), which has an FeO^T content (6.06 wt%) that is substantially lower than in Klyuchevskoy whole rocks (7.7-9.1 wt %, see Appendix A).

Electron microprobe analyses of olivines and melt inclusions were performed at the University of Oregon on a Cameca SX100 electron microprobe, using 15kV accelerating voltage, 10 nA beam current, and a 10 um spot size for olivines and a 15 um spot size for melt inclusions to minimize sodium loss. Corrections for sodium loss were done by fitting measured count rates vs. time with a best fit function, which can be used to extrapolate to time zero to determine actual Na_2O values. In order to obtain homogenized crystal-free matrix glass for electron microprobe analysis, samples of matrix glass were melted in the laser fluorination sample chamber under vacuum using a high intensity laser to melt all of the phases. These were then quenched by turning off power to the laser, and the glasses were prepared and analyzed on the electron microprobe.

Major and trace element whole-rock X-ray fluorescence (XRF) analyses for many samples were performed at the GeoAnalytical lab at Washington State University on a ThermoARL Advant'XP+ sequential X-ray fluorescence spectrometer. Some of the whole rock data that we report for lavas are values analyzed by XRF at the IFM-GEOMAR (Kiel, Germany) and were previously reported in Portnyagin et al. (2007a,b).

Concentrations of trace elements and H_2O in melt inclusions were determined by secondary-ion mass-spectrometry (SIMS) using a CAMECA ims4f at the Institute of Microelectronics (Yaroslavl', Russia). When analyzed, samples coated with a 30 nm

thick gold film were bombarded by a primary beam of O^{2-} ions. The area for analysis was first sputtered for 3 minutes with 70 μm diameter beam to remove surface contamination. For analysis, the beam was focused to a spot 10-20 μm. The primary-ion energy was 14.5 keV at 15–20 nA current. The secondary ions emitted from the sample were filtered by the high accelerating-voltage offset (–100 V, bandwidth ±50 V) and analyzed at a mass spectrometer resolution of $M/\Delta M = 300$ in pulse-counting mode. Counting time was dynamically corrected for each element and varied between 5 and 120 sec depending on current counting statistics. Single analyses are averaged from 5 cycles of measurements. Total analysis time varied from 50 to 70 min. Secondary ion intensities were normalized to $^{30}Si^{+}$ and converted to weight concentrations using calibration curves based on a set of well characterized natural and artificial glasses (Rocholl et al. 1997; Jochum et al. 2000; 2006). Correction of isobaric interferences was applied for Eu, Gd, Er and Yb following technique described in (Gurenko et al. 2005) and references therein). Accuracy and precision were estimated to be better than 10 % for all elements with concentrations above 1 ppm and 10 to 30% for concentrations 0.1-1 ppm and ~15 % for hydrogen. Detection limit for trace elements (100% analytical error) is estimated at 0.01-0.005 ppm. Background signal for $^{1}H^{+}$ converted to weight percent of water equivalent was 0.01-0.02 wt % as measured on nominally anhydrous olivine phenocrysts from highly depleted MORB from Sequeiros F.Z. Glass KL-2G (Jochum et al. 2000; 2006) was used as a daily monitor for trace element analyses. For melt inclusions analyzed for H_2O by both FTIR and SIMS (n=13), the average deviation between the two techniques is ±0.5 wt% H_2O. When the two inclusions showing the largest discrepancies between the two techniques are eliminated, the average deviation is ±0.36 wt% H_2O

References

Danyushevsky LV, McNeill AW, Sobolev AV (2002) Experimental and petrological studies of melt inclusions in phenocrysts from mantle-derived magmas: and overview of techniques, advantages and complications. Chemical Geology 183:5-24

Dixon JE, Pan V (1995) Determination of the molar absorptivity of dissolved carbonate in basanitic glass. American Mineralogist 80:1339-1342

Dixon JE, Stolper EM, Holloway JR (1995) An experimental study of water and carbon dioxide solubilities in mid-ocean ridge basaltic liquids. Part I: calibration and solubility models. Journal of Petrology 36/6:1607-1631

Jochum KP, Dingwell DP, Rocholl A, Stoll B, Hofmann AW, Becker S. and et al., (2000) The Preparation and Preliminary Characterisation of Eight Geological MPI-DING Reference Glasses for In-Situ Microanalysis, Geostandards Newsletter 24, 87-133.

Jochum KP et al., (2006) MPI-DING reference glasses for in situ microanalysis: New reference values for element concentrations and isotope ratios, Geochem. Geophys. Geosyst. 7(Q02008), doi:10.1029/2005GC001060.

Kelsey (1965) Calculation of the C.I.P.W. norm. Mineralogical magazine 34:276-282

Luhr JF (2001) Glass inclusions and melt volatile contents at Parícutin Volcano, Mexico. Contrib Mineral Petrol 142, 261–283.

Nichols ARL, Wysoczanski RJ (2007) Using micro-FTIR spectroscopy to measure volatile contents in small and unexposed inclusions hosted in olivine crystals. Chemical Geology 242(3-4):371-384

Ochs FA, Lange RA (1999) The density of hydrous magmatic liquids. Science 283:13414-1317

Rocholl ABE, Simon K, Jochum KP, Molzahn M, Pernicka E, Seufert M

Spettel B. and Stummeier J. (1997) Chemical characterization of NIST Silicate Glass Certified Reference Material SRM 610 by ICP-MS, TIMS, LIMS, SSMS, INAA, AAS and PIXE, Geostandards 21(1), 101-114.

Roggensack K (2001) Unraveling the 1974 eruption of Fuego volcano (Guatemala) with small crystals and their young melt inclusions. Geology 29, 911 –914.

Sobolev AV, Shimizu N (1993) Ultra-depleted primary melt included in an olivine from the Mid-Atlantic Ridge. Nature 363:151–154.

Appendix B Major and trace element analyses of rocks and melt inclusions of Klyuchvskoy

Table A1: Major and trace element analyses of tephra from Klyuchevskoy volcano analyzed in this study by XRF. See Figure 3 for sample localities.

Sample	KLV 4	KLV 5/1	KLV 5/3	KLV 5/4	KLV 5/5
Section	Cone D	KLV 05-05	KLV 05-05	KLV 05-05	KLV 05-05
Latitude	N56 08.527	N56 08.527	N56 08.527	N56 08.527	N56 08.527
Longitude	E160 48.054	E160 48.054	E160 48.054	E160 48.054	E160 48.054
Oxide, wt%		Un-normalized Major Elements (Weight %):			
SiO_2	53.27	52.36	52.83	53.46	53.00
TiO_2	0.91	0.98	1.04	1.03	1.03
Al_2O_3	16.95	17.56	18.10	18.08	17.15
FeO*	8.00	7.93	7.92	8.03	8.40
MnO	0.16	0.16	0.16	0.16	0.16
MgO	6.88	5.02	4.83	5.16	6.35
CaO	9.22	8.04	8.11	8.31	8.74
Na_2O	3.27	3.52	3.76	3.74	3.32
K_2O	0.76	0.93	0.77	0.85	0.71
P_2O_5	0.17	0.19	0.20	0.22	0.19
Sum	99.57	96.69	97.72	99.02	99.06
element, ppm		Un-normalized Trace Elements (ppm)			
Ni	65.3	35.5	25.5	27.3	51.2
Cr	197.1	52.5	37.5	38.4	119.8
Sc	30.6	24.3	26.6	26.1	29
V	242.8	235.9	257.1	251.7	245
Ba	264	380.2	274.2	297.3	240.7
Rb	12.2	14.9	10.4	12.5	10.7
Sr	328	338.2	319.9	359	318.9
Zr	78.9	88.6	91.7	92.9	92
Y	18.2	20.1	21.8	20.2	20.6
Nb	1.4	1.7	1.4	0.8	1.7
Ga	19.6	18.8	19.2	19.5	17.5
Cu	84.7	69.5	94.7	81.4	86.4
Zn	78.5	83	80.1	79.6	79.7
Pb	2.9	4	3.1	3.5	3
La	5.3	5.1	5	6.9	5.6
Ce	17.5	17.8	15.7	22.3	15.2
Th	2.4	3.4	3.1	3	1.8
Nd	12.8	11.7	11	14.4	11.6
K	0.632	0.773	0.638	0.702	0.593

Sample	KLV 5/6	KLV 5/8	KLV 5/10	KLV 5/12	KLV 5/13
Section	KLV 05-05	KLV 05-05	KLV 05-05	KLV 05-05	KLV 05-05
Latitude	N56 08.527	N56 08.527	N56 08.527	N56 08.527	N56 08.527
Longitude	E160 48.054	E160 48.054	E160 48.054	E160 48.054	E160 48.054
Oxide, wt%					
SiO_2	52.76	51.48	52.73	52.71	54.88
TiO_2	0.88	0.81	0.91	1.02	0.97
Al_2O_3	16.55	13.87	16.86	17.34	18.12
FeO*	8.20	8.55	8.39	8.91	7.72
MnO	0.16	0.17	0.16	0.17	0.15
MgO	7.67	11.30	6.70	5.83	4.92
CaO	9.30	9.78	9.13	8.80	8.13
Na_2O	3.04	2.36	2.87	2.94	3.47
K_2O	0.68	0.56	0.70	0.77	1.00
P_2O_5	0.16	0.14	0.15	0.17	0.18
Sum	99.40	99.01	98.62	98.66	99.55
element, ppm					
Ni	78.2	180.7	54.7	26.5	25.2
Cr	242.4	807.2	185.3	77.7	37.1
Sc	31.6	37.4	34.2	33.3	27.6
V	238.4	242.5	250.6	271.2	241.3
Ba	239.5	219.1	284.8	310.1	419.3
Rb	10.3	8.5	11.6	12	16.6
Sr	315.6	244.1	333.4	327.8	374.5
Zr	73.7	63.4	74.4	80.7	86.1
Y	18.1	16.7	17.1	22.2	20.1
Nb	1.6	1	1.8	1.3	2
Ga	16.4	15.3	18.7	17.4	18.9
Cu	75.2	76.9	68.2	41.4	39.2
Zn	75.1	73.1	78.2	83.6	81.2
Pb	3.3	2.4	3.6	2.8	4.3
La	2.6	3.8	5	5.3	5.3
Ce	13.5	14.6	14.9	10.6	18.3
Th	3.1	1.8	1.6	2.1	4.3
Nd	9.9	10.1	10.5	10.7	9.7
K	0.567	0.464	0.583	0.637	0.834

Sample	KLV 5/15	KLV 5/18a	KLV 5/19	KLV 5/20	KLV 5/22
Section	KLV 05-05	KLV 05-05	KLV 05-05	KLV 05-05	KLV 05-05
Latitude	N56 08.527	N56 08.527	N56 08.527	N56 08.527	N56 08.527
Longitude	E160 48.054	E160 48.054	E160 48.054	E160 48.054	E160 48.054
Oxide, wt%					
SiO_2	51.23	53.44	54.50	53.78	54.34
TiO_2	0.99	0.87	0.84	0.98	0.86
Al_2O_3	16.94	14.85	16.79	17.34	15.99
FeO*	9.12	8.34	7.91	8.31	8.12
MnO	0.18	0.16	0.16	0.16	0.16
MgO	6.36	9.60	7.06	6.24	6.80
CaO	9.03	8.84	8.55	8.86	8.85
Na_2O	2.68	2.62	2.95	2.89	2.89
K_2O	0.63	0.77	0.85	0.80	0.85
P_2O_5	0.16	0.17	0.18	0.15	0.18
Sum	97.30	99.67	99.79	99.51	99.05
element, ppm					
Ni	38.3	125.3	67.2	17.4	44.3
Cr	99.9	587.3	311.9	77.5	204.6
Sc	36.9	32.8	28	32.2	31.1
V	275.2	236	210	248	232.3
Ba	250.2	308.1	361.9	335.9	329.2
Rb	9.4	11.2	13.5	12.2	13
Sr	311.9	308.9	341.6	307.2	364.8
Zr	71.9	75	82.1	78.1	80.9
Y	20.1	19.3	20	20.2	17.8
Nb	2.2	1.4	1.3	1.1	1.3
Ga	18.6	16.3	18	17.8	18
Cu	87.7	30.7	26.9	20	57.9
Zn	80.3	79	91.7	84.2	78
Pb	2.7	3.5	3.3	3.5	3.1
La	4.3	3.3	5.8	5.5	4.5
Ce	16.1	13.2	17.7	10.3	16.8
Th	1.8	2.2	3	3.7	2.2
Nd	11.8	8.3	12.3	8.2	12.6
K	0.520	0.642	0.708	0.662	0.702

Sample	KLV 5/24	KLV 8	KLV 9	KLV 11/1	KLV 11/3
Section	KLV 05-05	Lepyoshka	nd	KLV 05-11	KLV 05-11
Latitude	N56 08.527	N56 08.992	N56 09.167	N56 09.167	N56 09.167
Longitude	E160 48.054	E160 47.710	E160 47.621	E160 47.621	E160 47.621
Oxide, wt%					
SiO_2	57.01	52.67	52.77	52.14	53.48
TiO_2	1.31	1.00	1.03	1.00	1.03
Al_2O_3	17.39	15.97	16.63	17.29	17.35
FeO*	7.27	8.78	8.86	8.74	8.90
MnO	0.13	0.17	0.17	0.17	0.17
MgO	2.64	7.28	6.86	6.62	5.90
CaO	6.35	9.52	9.29	9.30	9.00
Na_2O	3.61	2.76	2.83	3.03	3.05
K_2O	2.17	0.72	0.74	0.58	0.78
P_2O_5	0.61	0.16	0.17	0.15	0.16
Sum	98.49	99.02	99.34	99.03	99.84
element, ppm					
Ni	16.8	43.1	37.4	47.4	25.5
Cr	15.6	199	145.6	142.7	66.6
Sc	21.5	37	35.1	33.8	33.9
V	222.9	272.1	271.7	270.6	277.6
Ba	725.9	292.1	313.4	219.6	306.2
Rb	62.2	10.3	11.1	7.7	12.3
Sr	320.7	302.9	316.1	320.6	333.6
Zr	298.2	76.4	78.8	74	78.9
Y	42.5	21.9	21.4	20.3	21
Nb	6	1.8	1.6	1.5	1.4
Ga	20.8	16	19	17.4	19.2
Cu	203.2	42.8	40.1	73.8	42.4
Zn	88.4	81.8	83.6	80.4	84.3
Pb	9.5	3.6	2.8	1.2	3.4
La	22.8	7	6.7	1.7	5.7
Ce	62.3	17.2	13.1	12.2	19.1
Th	8.2	3.4	2.4	1.8	3.4
Nd	39.3	11.5	9.3	9.7	11.1
K	1.805	0.595	0.611	0.484	0.650

Sample	KLV 11/5	84093/1	84093/5	300/48	300/63
Section	KLV 05-11	840-93	840-93	300-75	300-75
Latitude	N56 09.167	nd	nd	nd	nd
Longitude	E160 47.621	nd	nd	nd	nd
Oxide, wt%					
SiO_2	54.56	53.66	53.92	52.98	53.10
TiO_2	0.97	0.91	1.06	1.03	1.03
Al_2O_3	17.90	16.97	18.17	17.04	17.23
FeO*	7.67	8.34	8.25	8.85	8.35
MnO	0.15	0.16	0.16	0.17	0.16
MgO	4.98	6.77	5.09	5.96	6.28
CaO	8.12	8.68	8.30	8.89	8.80
Na_2O	3.42	3.24	3.78	2.94	3.32
K_2O	1.00	0.81	0.77	0.77	0.71
P_2O_5	0.18	0.17	0.20	0.17	0.19
Sum	98.94	99.71	99.69	98.79	99.17
element, ppm					
Ni	25.1	55.7	28.5	27.6	49.3
Cr	40.9	133.7	34.1	73.3	128.3
Sc	27.3	28.9	27.3	32.9	29.5
V	238.3	237.7	263.3	275.4	250.6
Ba	415.3	334.4	272.5	306.2	241
Rb	16.3	12.8	12.6	12.1	10.2
Sr	369.7	317.5	320	326.1	319.5
Zr	85.5	79.4	92.4	79.2	92.5
Y	19.8	19.4	21.7	20.8	21
Nb	1.4	0.6	1.8	1.2	1.3
Ga	18.7	16.4	20.5	17.9	19.3
Cu	35.9	58.3	84.8	39.6	84.4
Zn	81.7	80.7	79.8	83.9	80
Pb	3.7	2.9	3.5	3.2	3.8
La	6.3	3.6	5.8	6.7	4.1
Ce	16.9	14.9	17.4	15.1	14.7
Th	2.8	3.1	2.5	3	1.5
Nd	12.9	8.8	14	10.2	12
K	0.833	0.674	0.635	0.640	0.592

Sample	300/19
Section	tephra
Latitude	nd
Longitude	nd

Oxide, wt%	
SiO_2	55.42
TiO_2	1.33
Al_2O_3	17.39
FeO*	8.09
MnO	0.19
MgO	2.62
CaO	7.30
Na_2O	3.76
K_2O	2.20
P_2O_5	0.57
Sum	98.87

Table A2: Composition of melt inclusions and their host olivines in tephra from Klyuchevskoy volcano
Major elements and Cl, S, F, were measured by the electron microprobe, trace elements were measured by the ion microprobe; quoted iron values are calculated from FeO* analyses by taking Fe2O3/FeO=0.15
MI Corrected for Post-entrapment Crystallization (PEC) nd: no data

Italicized values are analyses in which the probe beam accidently included both olivine and the melt inclusion glass

EMPA									
Sample	84093/5	KLV 4	KLV 4	KLV 4	KLV 4	84093/1	84093/1	KLV 5/8	KLV 5/8
inclusion	4a	5A	5B	4B	1	3	4	1	2
wt%									
SiO_2	52.27	50.60	50.59	50.63	56.58	*49.11*	55.45	50.78	50.63
Al_2O_3	17.57	16.07	15.87	15.65	14.58	*10.42*	16.42	17.46	15.65
Fe_2O_3	1.49	1.33	1.32	1.40	1.60	*2.45*	1.47	1.36	1.40
FeO	8.43	7.27	7.45	7.92	8.16	*12.51*	7.50	7.45	7.92
MgO	5.10	7.61	7.80	8.35	4.71	*17.09*	5.23	7.39	8.35
CaO	8.51	11.78	11.76	10.72	8.05	*4.40*	8.01	10.63	10.72
Na_2O	4.06	3.08	3.04	3.23	3.28	*2.20*	3.45	2.98	3.23
K_2O	0.77	0.63	0.63	0.67	1.16	*0.74*	0.90	0.57	0.67
TiO_2	1.06	0.91	0.95	0.87	1.56	*0.86*	1.10	0.85	0.87
MnO	0.17	0.17	0.09	0.09	0.19	*0.24*	0.20	0.17	0.09
P_2O_5	0.21	0.19	0.17	0.18	0.25	*0.18*	0.23	0.16	0.18
S	0.15	0.21	0.20	0.20	0.01	*0.01*	0.05	0.12	0.20
Cl	0.06	0.07	0.06	0.07	0.05	*0.03*	0.04	0.05	0.07
F	0.16	0.07	0.07	0.04	nd	*0.01*	0.08	0.03	0.04
H_2O FTIR wt%	3.76	2.24	2.21	2.75	0.84	2.79	3.87	2.49	1.85
CO_2 FTIR ppm	1067	<50ppm	<50ppm	<50ppm	<50ppm	<50ppm	<50ppm	520	657
Fo Ol host	78.2	86.2	86.2	86.2	76.9	76.2	77.6	85.5	85.1
PEC %	0.0	3.3	5.1	5.4	0.0	0.0	0.0	3.4	5.4

EMPA Sample inclusion wt%	KLV 5/8 3	KLV 5/8 4A	KLV 5/8 4B	KLV 5/8 4C	300/63 1	300/63 2	300/63 5	300/63 5B	300/63 6
SiO_2	50.45	51.57	52.34	nd	53.36	53.16	52.31	51.94	51.24
Al_2O_3	14.99	14.99	15.92	nd	17.29	17.65	17.94	17.99	18.48
Fe_2O_3	1.31	1.24	1.15	nd	1.48	1.45	1.48	1.53	1.61
FeO	6.86	8.20	7.07	nd	7.61	7.46	7.55	7.82	8.22
MgO	9.13	10.40	9.08	nd	5.59	5.49	5.64	6.02	5.67
CaO	12.94	8.86	9.91	nd	9.04	8.81	9.22	8.89	9.08
Na_2O	2.59	2.70	2.59	nd	3.39	3.54	3.54	3.57	3.36
K_2O	0.42	0.67	0.58	nd	0.66	0.69	0.69	0.75	0.61
TiO_2	0.82	0.97	0.95	nd	1.12	1.20	1.18	1.12	1.15
MnO	0.12	0.18	0.14	nd	0.14	0.18	0.13	0.11	0.23
P_2O_5	0.12	0.15	0.18	nd	0.20	0.18	0.21	0.24	0.20
S	0.25	0.02	0.02	nd	0.16	0.16	0.16	0.17	0.22
Cl	0.06	0.05	0.05	nd	0.05	0.06	0.05	0.06	0.07
F	0.00	nd	nd	nd	0.02	0.07	0.07	-0.05	0.03
H_2O FTIR wt%	3.92	0.40	nd	1.09	1.76	3.40	3.25	3.25	7.09
CO_2 FTIR ppm	528	<50ppm	<50ppm	<50ppm	<50ppm	<50ppm	887	887	<50ppm
Fo Ol host	88.0	88.3	88.4	nd	80.9	80.8	80.5	80.5	79.9
PEC %	2.4	15.6	7.7	nd	0.8	0.4	0.0	0.0	0.0

EMPA									
Sample inclusion wt%	300/63 7	300/63 8	300/63 10	300/63 11	KLV 5/18a 1	KLV 5/18a 3	KLV 5/18a 4	KLV 5/18a 5	KLV 5/18a 6
SiO_2	52.88	52.69	53.12	53.51	52.26	53.09	52.41	53.49	50.79
Al_2O_3	17.86	18.42	17.61	17.29	18.50	17.80	18.33	17.44	18.92
Fe_2O_3	1.43	1.43	1.51	1.33	1.43	1.27	1.29	1.00	1.41
FeO	7.32	7.42	7.68	7.44	7.56	8.19	6.84	5.16	7.70
MgO	5.42	5.37	5.72	5.68	5.79	6.29	5.07	5.55	5.77
CaO	9.00	9.01	8.48	9.00	8.88	8.85	10.25	12.38	9.64
Na_2O	3.76	3.59	3.66	3.49	2.76	1.80	3.14	3.15	2.42
K_2O	0.74	0.64	0.72	0.63	0.99	0.98	1.02	1.04	0.82
TiO_2	1.16	0.85	1.01	1.03	1.09	1.05	1.00	0.93	1.89
MnO	0.12	0.21	0.17	0.17	0.15	0.14	0.14	0.11	0.16
P_2O_5	0.21	0.22	0.21	0.19	0.23	0.21	0.21	0.25	0.17
S	0.16	0.18	0.15	0.15	0.19	0.19	0.20	0.30	0.15
Cl	0.05	0.06	0.05	0.05	0.08	0.09	0.08	0.13	0.06
F	0.04	-0.09	0.07	0.04	0.09	0.06	0.01	0.03	0.09
H_2O FTIR wt%	4.84	3.10	5.32	4.37	3.82	1.00	2.21	2.91	4.20
CO_2 FTIR ppm	1008	780	1269	<50ppm	1036	703	804	651	1884
Fo Ol host	81.3	81.1	80.8	81.9	82.0	82.0	81.5	86.4	81.7
PEC %	0.0	0.4	0.0	2.9	1.4	8.4	1.6	0.5	2.7

SIMS Sample inclusion ppm	84093/5 4a	KLV 4 5a	KLV 4 5b	KLV 4 4b	KLV 4 1	84093/1 3	84093/1 4	KLV 5/8 1	KLV 5/8 2
Ba	209	209	220	149	361	nd	377	217	215
U	0.28	0.26	0.23	0.22	0.48	nd	0.43	0.21	0.30
Th	0.34	0.34	0.33	0.30	0.78	nd	0.53	0.27	0.27
K	5463	4806	5266	4377	9602	nd	8027	5616	4728
Cl	nd	nd	nd	nd	nd	nd	429	486	nd
H2O, wt%	4.45	2.05	2.67	3.45	1.80	nd	3.94	2.49	2.12
Nb	1.53	1.46	1.58	1.07	2.78	nd	1.97	1.66	1.32
La	4.89	4.81	4.92	3.35	7.78	nd	6.18	4.09	3.92
Be	0.67	0.34	0.42	0.45	0.84	nd	0.71	0.42	0.52
Ce	12.95	12.46	12.45	9.01	20.41	nd	16.47	10.39	10.80
Sr	255	293	311	217	246	nd	280	285	259
Nd	9.17	9.60	10.28	7.02	15.33	nd	11.39	8.15	8.91
Zr	75	61	65	49	118	nd	85	61	62
B	17.06	10.36	12.80	13.93	19.62	nd	16.18	16.29	15.48
Sm	2.61	3.13	3.04	2.09	4.13	nd	2.98	2.52	2.90
Eu	0.76	0.96	1.24	0.68	1.40	nd	1.12	0.84	0.97
Ti	6007	4115	5338	5344	8352	nd	6367	5473	6459
Dy	2.98	3.18	3.52	2.34	4.77	nd	3.46	2.71	3.23
Y	18.92	17.91	20.02	14.19	28.86	nd	20.70	18.14	20.52
Li	8.14	6.14	6.42	6.98	12.83	nd	10.48	7.07	6.75
Yb	1.85	2.12	2.31	1.52	3.02	nd	2.27	1.93	2.13
F	350	228	295	0.03	0.02	nd	0.03	0.04	0.03
V	247	268	288	226	355	nd	271	265	332
Cr	59	231	215	248	116	nd	69	134	104
Gd	3.13	2.82	3.54	2.76	5.02	nd	3.65	2.23	2.35
Er	1.88	2.35	2.31	1.61	3.47	nd	2.32	1.98	2.51
Hf	2.06	2.26	2.23	1.52	3.31	nd	2.33	1.90	1.79
Pb	1.83	1.54	2.28	1.45	4.04	nd	2.86	3.65	1.89

SIMS Sample inclusion ppm	KLV 5/8 3	KLV 5/8 4A	KLV 5/8 4B	KLV 5/8 4C	300/63 1	300/63 2	300/63 5	300/63 5B	300/63 6
Ba	195	260	215	135	nd	219	202	nd	nd
U	0.18	0.30	0.30	0.24	nd	0.29	0.22	nd	nd
Th	0.27	0.38	0.27	0.22	nd	0.34	0.39	nd	nd
K	4189	6120	5120	3070	nd	6108	5566	nd	nd
Cl	602	nd	nd	nd	nd	574	503	nd	nd
H2O, wt%	3.24	nd	nd	nd	nd	3.29	3.77	nd	nd
Nb	1.38	1.68	1.50	0.92	nd	1.93	1.83	nd	nd
La	3.81	4.87	4.12	2.84	nd	5.02	4.82	nd	nd
Be	0.39	nd	nd	nd	nd	0.60	0.59	nd	nd
Ce	10.30	13.66	11.08	8.12	nd	12.90	12.67	nd	nd
Sr	249	271	248	212	nd	285	270	nd	nd
Nd	8.73	9.63	8.54	6.35	nd	9.82	9.03	nd	nd
Zr	60	70	63	43	nd	79	78	nd	nd
B	11.96	nd	nd	nd	nd	18.69	15.07	nd	nd
Sm	2.83	2.61	2.78	1.73	nd	2.96	2.72	nd	nd
Eu	0.89	0.86	0.90	0.75	nd	0.87	0.88	nd	nd
Ti	5613	nd	nd	nd	nd	5910	5905	nd	nd
Dy	3.14	3.29	2.92	2.35	nd	3.13	2.99	nd	nd
Y	20.14	20.05	17.46	14.32	nd	19.07	17.94	nd	nd
Li	5.38	nd	nd	nd	nd	7.73	7.17	nd	nd
Yb	2.25	2.37	1.76	1.81	nd	1.99	2.06	nd	nd
F	0.03	nd	nd	nd	nd	0.03	0.03	nd	nd
V	305	278	265	263	nd	255	239	nd	nd
Cr	204	100	136	255	nd	95	74	nd	nd
Gd	2.30	3.02	2.78	1.97	nd	3.19	2.74	nd	nd
Er	2.12	2.46	2.02	1.74	nd	2.06	1.94	nd	nd
Hf	1.91	2.01	1.81	1.50	nd	2.20	2.03	nd	nd

Pb	1.38	2.83	1.91	1.35	nd	2.17	2.02	nd	nd

SIMS									
Sample inclusion ppm	300/63 7	300/63 8	300/63 10	300/63 11	KLV 5/18a 1	KLV 5/18a 3	KLV 5/18a 4	KLV 5/18a 5	KLV 5/18a 6
Ba	205	203	nd	nd	nd	nd	nd	nd	nd
U	0.26	0.28	nd	nd	nd	nd	nd	nd	nd
Th	0.37	0.38	nd	nd	nd	nd	nd	nd	nd
K	5740	5559	nd	nd	nd	nd	nd	nd	nd
Cl	491	575	nd	nd	nd	nd	nd	nd	nd
H_2O, wt%	3.24	3.41	nd	nd	nd	nd	nd	nd	nd
Nb	1.95	2.18	nd	nd	nd	nd	nd	nd	nd
La	5.06	5.35	nd	nd	nd	nd	nd	nd	nd
Be	0.62	0.65	nd	nd	nd	nd	nd	nd	nd
Ce	13.09	12.96	nd	nd	nd	nd	nd	nd	nd
Sr	276	277	nd	nd	nd	nd	nd	nd	nd
Nd	9.59	9.74	nd	nd	nd	nd	nd	nd	nd
Zr	80	84	nd	nd	nd	nd	nd	nd	nd
B	15.79	16.76	nd	nd	nd	nd	nd	nd	nd
Sm	2.73	2.41	nd	nd	nd	nd	nd	nd	nd
Eu	0.90	0.87	nd	nd	nd	nd	nd	nd	nd
Ti	6134	6339	nd	nd	nd	nd	nd	nd	nd
Dy	2.95	3.01	nd	nd	nd	nd	nd	nd	nd
Y	19.38	20.73	nd	nd	nd	nd	nd	nd	nd
Li	7.09	7.97	nd	nd	nd	nd	nd	nd	nd
Yb	1.85	2.06	nd	nd	nd	nd	nd	nd	nd
F	0.02	0.03	nd	nd	nd	nd	nd	nd	nd
V	243	259	nd	nd	nd	nd	nd	nd	nd
Cr	87	59	nd	nd	nd	nd	nd	nd	nd
Gd	2.65	2.81	nd	nd	nd	nd	nd	nd	nd
Er	2.12	1.98	nd	nd	nd	nd	nd	nd	nd
Hf	2.35	2.20	nd	nd	nd	nd	nd	nd	nd
Pb	1.71	2.01	nd	nd	nd	nd	nd	nd	nd